Targeted pharmacological therapy restores β-cell function for diabetes remission

Stephan Sachs[1,2,11,14]*, Aimée Bastidas-Ponce[1,11,14]*, Sophie Tritschler[1,3,11,14]*, Mostafa Bakhti[1,14], Anika Böttcher[1], Miguel A. Sánchez-Garrido[2], Marta Tarquis-Medina[1,11], Maximilian Kleinert[2,4], Katrin Fischer[2], Sigrid Jall[2], Alexandra Harger[2], Erik Bader[1], Sara Roscioni[1], Siegfried Ussar[5,11,14], Annette Feuchtinger[6], Burcak Yesildag[7], Aparna Neelakandhan[7], Christine B. Jensen[8], Marion Cornu[8], Bin Yang[9], Brian Finan[9], Richard DiMarchi[9,10], Matthias H. Tschöp[2,11,14], Fabian Theis[3,11,14,#], Susanna M. Hofmann[1,12,14,#], Timo D. Müller[2,13,14#], Heiko Lickert[1,11,14,15#]

[1]Institute of Diabetes and Regeneration Research, Helmholtz Diabetes Center**,** Helmholtz Center Munich, 85764 Neuherberg, Germany.

[2]Institute of Diabetes and Obesity, Helmholtz Diabetes Center**,** Helmholtz Center Munich, 85764 Neuherberg, Germany.

[3]Institute of Computational Biology, Helmholtz Zentrum München, 85764 Neuherberg, Germany.

[4]Section of Molecular Physiology, Department of Nutrition, Exercise and Sports, University of Copenhagen, Copenhagen, 2100, Denmark.

[5]RG Adipocytes & Metabolism, Institute for Diabetes & Obesity, Helmholtz Diabetes Center, Helmholtz Center Munich, 85764 Neuherberg, Germany.

[6]Research Unit Analytical Pathology, Helmholtz Center Munich, 85764, Neuherberg, Germany.

[7]InSphero AG, Schlieren, Switzerland

[8]Global Drug Discovery, Novo Nordisk A/S, Maaloev, Denmark

[9]Novo Nordisk Research Center Indianapolis, Indianapolis, Indiana, USA.

[10]Department of Chemistry, Indiana University, Bloomington, Indiana. USA.

[11]Technical University of Munich, School of Medicine, 80333 Munich, Germany.

[12]Medizinische Klinik und Poliklinik IV, Klinikum der Ludwig Maximilian Universität, Munich, Germany.

[13]Department of Pharmacology and Experimental Therapy, Institute of Experimental and Clinical Pharmacology and Toxicology, Eberhard Karls University Hospitals and Clinics, Tübingen, Germany.

[14]German Center for Diabetes Research (DZD), 85764 Neuherberg, Germany.

[15]Lead contact

*These authors contributed equally to this work: Stephan Sachs, Aimée Bastidas-Ponce, and Sophie Tritschler

[#]Authors for correspondence: Fabian Theis, Susanna M. Hofmann, Timo D. Müller, and Heiko Lickert (heiko.lickert@helmholtz-muenchen.de)

Summary

Dedifferentiation of insulin-secreting β-cells in the islet of Langerhans has been proposed as a major mechanism of β-cell dysfunction in type 1 (T1D) and type 2 diabetes (T2D). However, if and how dedifferentiated β-cells can be directly targeted by pharmacological intervention for diabetes remission is still undefined. Here we established the multiple low dose streptozotocin (mSTZ) model of murine diabetes as a model for β-cell dedifferentiation and examine paths and mechanisms of this process. Furthermore, we performed a benchmark study to test treatments that can restore β-cell function. For this we stratified seven cohorts of severely diabetic mice and treated them daily for 100 days with single and combinatorial pharmacology. Single cell RNA sequencing (scRNA-seq) of islet and remaining insulin-positive cells after initial mSTZ-mediated β-cell destruction and long-term hyperglycemia identified many novel markers and pathways associated with β-cell dedifferentiation and dysfunction. Insulin treatment triggers insulin receptor pathway activation and RNA polymerase II transcription in β-cells to restore maturation and function for diabetes remission, beside relieving β-cells from glucotoxic stress. We further show that a stable Glucagon-like peptide-1 (GLP-1)/estrogen conjugate enables the safe and selective delivery of the nuclear hormone cargo to β-cells. This decreases the daily insulin requirement by 60%, enabled the estrogen-specific activation of the endoplasmic-reticulum-associated protein degradation (ERAD) system and increased murine β-cell survival, maturation and functionality. Importantly, this GLP-1 peptide-based estrogen conjugate also protected human β-cells against cytokine-induced stress and dysfunction. Neither estrogen nor GLP-1 alone had stress or disease modifying effects in these models. Not only does our study describe paths and processes of β-cell dedifferentiation, but also demonstrates the potential and mechanisms of single and combinatorial drug treatments to revers diabetes progression by targeting dedifferentiated β-cells.

59 The progressive loss or dysfunction of insulin-producing β-cell mass ultimately leads to T1D or T2D,
60 respectively[1]. Current pharmacological treatments do not stop the decline of β-cell function and number
61 leading to glucose excursions and, eventually, to devastating micro- and macrovascular complications.
62 Hence, the ideal treatment should be initiated when first diabetic symptoms appear and protect or
63 regenerate glucose-sensing and insulin-secreting β-cells for optimal blood glucose regulation to prevent
64 secondary complications. Recently, T1D progression has been halted by anti-CD3 immunotherapy for
65 2 years[2], but it will be important to test whether additional β-cell regenerative therapy can further or
66 permanently delay onset of diabetes. Intensive insulin therapy at disease onset has been shown to
67 partially restore β-cell function that slows disease progression in T1D and T2D patients (The Diabetes
68 Control and Complications Trial Research Group, 1998)[3–6]. Despite similar glycemic control, early
69 intensive insulin treatment in T2D patients better preserves β-cell function compared to oral anti-diabetic
70 drugs, suggesting additional glucose independent beneficial effects[7,8]. Thus, understanding mechanisms
71 of β-cell dysfunction and pharmacological replenishment are urgently needed to stop or reverse diabetes
72 progression and improve patients' therapy. Dedifferentiation of β-cells has been observed in genetic
73 mouse models of T1D and T2D as well as diabetic patients, which is characterized by the loss of the
74 expression of key maturation markers (e.g. *Glut2* and *Ucn3*) and an impaired insulin secretion thereby
75 contributing to β-cell dysfunction and hyperglycemia[9–13]. To investigate whether dysfunctional β-cells
76 under hyperglycemic conditions can be targeted pharmacologically to restore β-cell function, we
77 explored the model of mSTZ-induced diabetes. STZ specifically ablates β-cells[14], but when injected in
78 multiple low doses, some residual β-cells can survive[15]. Furthermore, the absence of genetic lesions and
79 autoimmunity in the mSTZ model allows the investigation of the fate of those remaining β-cells and the
80 effect of pharmacological treatment on β-cell protection and regeneration.
81

Insulin restores β-cell function

Ten days after the last mSTZ injection, mice were severely hyperglycemic (Extended Data Fig. 1a) and showed an impaired islet architecture (Extended Data Fig. 1b) with markedly decreased β-cell numbers (Extended Data Fig. 1b, c). Proliferation of remaining β-cells was unchanged (Extended Data Fig. 1d), whereas β-cell apoptosis was significantly increased in mSTZ-treated mice (Extended Data Fig. 1e) and accompanied by a loss of identity and function (Extended Data Fig. 1f, g, h). Hence, at this time point (diabetes onset), we initiated a permanent drug treatment over 100 days, when a fraction of dysfunctional β-cells were still remaining (Fig. 1a). Vehicle treated mSTZ mice remained diabetic over the length of the study, suggesting that the residual β-cell functionality or endogenous β-cell regeneration[16,17] is insufficient to maintain or restore sufficient glucose homeostasis (Fig. 1b-f). To correct the insulin deficiency in mSTZ mice, we treated diabetic mice with a long-acting pegylated insulin analog (PEG-insulin, once daily; M&M), which improved glycemia (Fig. 1b), increased C-peptide levels (Fig. 1c), improved islet structure (Fig. 1d) and increased the number of insulin-positive cells (Fig. 1e, f). This shows functional β-cell recovery upon glycemia normalization, which extents findings from insulin treatment in genetic mouse models[18,19]. However, the risk of hypoglycemia and unwanted weight gain are undesirable hallmarks of insulin therapy, thus alternative pharmacological approaches are required to mitigate these liabilities.

GLP-1/estrogen and insulin polypharmacotherapy

Estrogen and GLP-1 have been repeatedly implicated in the treatment of diabetes due to insulinotropic and β-cell protective effects in preclinical studies[20,21]. Chemically optimized GLP-1 analogs profoundly improve glucose and body weight management in obese and T2D patients[22,23]. However, severe gynecological, oncogenic and mitogenic side effects precludes chronic estrogen use as a drug for diabetes and, up-to-date, GLP-1 analogs failed to preserve β-cell function and mass in obese and diabetic humans[21,24].

To circumvent estrogen's gynecological, oncogenic and mitogenic actions, we recently designed and evaluated a stable GLP-1/estrogen conjugate, which reversed the metabolic syndrome in diet-induced obese male and female mice[25]. Here, we used the GLP-1/estrogen conjugate to test whether the specific

delivery of estrogen into GLP-1R expressing β-cells could restore β-cell functionality. GLP-1/estrogen treatment for 100 days was more efficacious to decrease fasting glucose (Fig. 1b) and increase fasting C-peptide (Fig. 1c) and insulin levels (Extended Data Fig. 2a) than either of the mono-components (estrogen or GLP-1 alone). Moreover, only GLP-1/estrogen treatment improved pancreatic islet architecture (Fig. 1d) and increased β-cell number (Fig. 1e, f). These effects were independent of body weight loss (Extended Data Fig. 2b).

Polypharmacotherapy holds the potential to simultaneously activate redundant or additive pathways to enhance efficacy while enabling reduced dosing of the individual components and consequently reduce the risk of unwanted side effects[26]. We tested the combination of insulin and GLP-1/estrogen to investigate a triple pharmacological approach to enhance the efficacy of both compounds, and particularly lessen the amount of insulin required. The combination therapy normalized glycemia (Fig. 1b) and increased C-peptide levels (Fig. 1c). Furthermore, the combination therapy displayed a superior effect compared to the insulin alone to limit weight gain (Extended Data Fig. 2b), normalize glucose tolerance (Extended Data Fig. 2c), increase pancreatic insulin content (Extended Data Fig. 2d) and increase β-cell number (Fig. 1e, f). Importantly, we were able to reduce the insulin dose by 60% (10 nmol/kg) compared to the insulin monotreatment (25 nmol/kg) and still achieve superior therapeutic outcomes, which reduces the risk of hypoglycemia and unintended weight gain.

To test whether treatment induced improvements on glucose and islet homeostasis are maintained, we switched a group of mice after 12 weeks of GLP-1/estrogen treatment to two additional weeks of vehicle injections. Positive effects of GLP-1/estrogen treatment to reduce fasting glycemia (Fig. 2a), increase fasting C-peptide levels (Fig. 2b), and enhance the β-cell maturation state (Fig. 2c, d) were sustained after these two weeks, supporting the notion of preserved islet cell function even after treatment cessation.

GLP-1/estrogen targets β-cells

We next wanted to confirm the absence of systemic toxicity related to the estrogen component of the GLP-1/estrogen conjugate, a pre-requisite for clinical use. To that end, we investigated whether GLP-1/estrogen (doses up to 10x higher than generally used in mouse experiment, and at least 1000x plasma

138 estradiol exposure as compared to women on hormone replacement therapy[27]) increased uterus weight
139 in ovariectomized (OVX) rats after two weeks of treatment (M&M, Extended Data Fig. 3a). In contrast
140 to estrogen alone, no treatment-related effect was observed with the GLP-1/estrogen conjugate
141 (Extended Data Fig. 3b), consistent with previously reported results in OVX mice[25].
142 To confirm β-cell-specific targeting of the GLP-1/estrogen conjugate, we used a double knock-in
143 fluorescent reporter mouse model (Foxa2-Venus Fusion (FVF) x Pdx1-BFP (blue fluorescent protein)
144 Fusion (PBF); FVFPBF^{DHom})[28], which allows α- and β-cell sorting (Extended Data Fig. 3c, d). Male
145 FVFPBF^{DHom} mice develop maturity onset diabetes of the young (MODY) due to reduced Pdx1 levels
146 in islets accompanied by hyperglycemia, reduced β-cell number and impaired islet architecture at
147 weaning age[28]. In this genetic diabetes model, none of the therapies improved glycemia after four weeks
148 of treatment (Extended Data Fig. 3e, f). These results suggest that β-cell function cannot be restored
149 pharmacologically in the presence of the genetically-induced β-cell lesions in the FVFPBF^{DHom} mice.
150 However, the GLP-1/estrogen conjugate, but not the monoagonists, specifically increased β-cell
151 granularity of FVFPBF^{DHom} mice, which shows that the conjugate selectively targets β-cells (Extended
152 Data Fig. 3g).
153
154 **GLP-1/estrogen improves human β-cell function**
155 To provide human relevance of the findings, we tested GLP-1/estrogen and the monoagonists in human
156 micro-islets in the absence or presence of β-cell stressors (cytokine cocktail, M&M). After acute
157 compound exposure, GLP-1/estrogen was more potent than either of the individual components to
158 increase glucose-stimulated insulin secretion (GSIS) from human micro-islets (Fig. 3a). We next
159 exposed the human micro-islets to cytokines to determine whether the beneficial effects of GLP-
160 1/estrogen protect against stress-induced impairment of β-cell functionality (Fig. 3b). Seven-day
161 treatment with GLP-1/estrogen enhanced GSIS, exceeding effects seen with either of the
162 monocomponents (Fig. 3b). Moreover, only GLP-1/estrogen treatment increased total insulin content of
163 cytokine exposed human micro-islets (Fig. 3c). This was independent of changes in total ATP content
164 (Extended Data Fig. 4a) and caspase luciferase activity (Extended Data Fig. 4b), suggesting that
165 compound treatment improved functionality, but not cell survival of human micro-islets. These results

show that GLP-1/estrogen is superior to both monoagonists to improve β-cell function in homeostasis and upon cytokine stress in mouse and human.

β-cell heterogeneity in homeostatic and healthy mice

To elucidate the molecular mechanisms underlying β-cell failure in mSTZ diabetes and β-cell recovery after the different therapeutic approaches, we performed scRNA-seq of isolated islets from mice that responded to treatment (Extended Data Fig. 5).

In normal islet homeostasis, we identified the four main endocrine cell subtypes, α-, β-, δ-, and PP-cells by unbiased graph-based clustering. Clusters were annotated based on predominant endocrine hormone expression of glucagon (Gcg), insulin (Ins), somatostatin (Sst), and pancreatic polypeptide (PP), respectively (Extended Data Fig. 6a, b, M&M). For each of the four endocrine subtypes we identified a specific marker gene signature (Supplemental Table 1, M&M). Refined clustering of insulin-positive cells revealed two main β-cell subpopulations: β1 and β2 (Extended Data Fig. 6c, M&M). Single cell trajectory inference[29,30] suggests a continuum of transcriptional states rather than discrete phenotypes within β-cells and a transition between β1 and β2 subpopulations (Extended Data Fig. 6d, M&M). We found a progressive increase of β-cell maturation markers (e.g. *Ins1*, *Ins2*, and *Ucn3*[9]), genes of the secretion machinery (*G6pc2*, *Sytl4*, and *Slc2a2*) and a concomitant decrease of β-cell immaturity (*Mafb*[31]) as well as pan-endocrine lineage markers (*Chga* and *Chgb*) along the pseudotime trajection from β2- to β1-cells (Extended Data Fig. 6d and Supplemental Table 2). Transcription factors (TFs) associated with β-cell identity (e.g. *Pdx1*, *Nkx6.1* and *NeuroD1*) were unchanged (Extended Data Fig. 6d). The β2-cell cluster was characterized by a downregulation of genes involved in insulin secretion, oxidative phosphorylation and cell-cycle inhibition as well as an upregulation of cAMP and WNT signaling (Extended Data Fig. 6e), suggestive for a more immature and/or proliferative state of β2-cells[32]. Consistently, we found an upregulation of cell cycle-associated genes, such as e.g. *Ki67* and *Cdk1* in the immature β2 subpopulation and accordingly, 16/403 of the β2-cells, whereas only 2/5319 of the mature β1-cells were classified as cycling (Extended Data Fig. 6f (M&M)). Together, this confirms the co-existence of mature (β1) and immature and/or proliferative β-cells (β2) in healthy mouse islets[32,33]. In addition, we found subpopulations of polyhormonal cells that could be distinguished from

doublets and ambient RNA, common problems of the scRNA-seq technology (Extended Data Fig. 6g, h, M&M).

β-cell dedifferentiation on single cell level

To get a deeper understanding of the cell autonomous and non-cell autonomous effects underlying chemical β-cell ablation in the islet cell niche, we performed a scRNA-seq survey of diabetic islets after 100 days of persistent hyperglycemia. Unsupervised clustering and embedding of the scRNA-seq data revealed altered endocrine subtype composition and cell-intrinsic gene expression profiles indicated by shifted cell cluster location in the UMAP space of mSTZ-diabetic compared to healthy mice (Fig. 4a and Supplemental Table 3). Especially, there was a 3-fold decrease of the proportion of β-cells and mSTZ β-cells formed an own cluster clearly distinct from healthy β-cells (Fig. 4a). In contrast to β-cells, only few transcriptional changes were detected for α-, δ-, and PP-cells (Extended Data Fig. 7a-f and Supplemental Table 3). We next sought to describe the progression from healthy to dysfunctional β-cells and its associated gene expression changes using single cell trajectory inference. Cells were ordered based on a cell-to-cell distance metric calculated using the concept of diffusion pseudotime (M&M). We identified a cellular trajectory where cells transitioned from mature to immature to mSTZ β-cells (Fig. 4b). Remaining mSTZ β-cells expressed low *Ins1* and/or *Ins2* mRNA and also showed sustained low expression of β-cell identity TFs, such as *Pdx1*, *Nkx2.2*, *Nkx6.1*, *Pax6*, *Isl1*, and *NeuroD1*[34–39] (Fig. 4b). Pathways associated with β-cell maturity and functionality were downregulated, while ER stress and oxidative phosphorylation pathways were upregulated in remaining mSTZ β-cells, altogether indicative of an ER stress response and β-cell dysfunction (Fig. 4c and Supplemental Table 3). Along this trajectory, key markers of β-cell maturity and functionality gradually decreased concomitant with an increase of the very few known markers of β-cell immaturity and dedifferentiation (e.g. Aldh1a3[40] and Gastrin[41]) (Fig. 4b, d). Strikingly, our single cell analysis uncovered a large number of upregulated genes and pathways in mSTZ β-cells that are not expressed at all or only subtly expressed in mature, functional murine β-cells (Fig. 4e). We confirmed increased expression of e.g. Cck and Slc5a10 by immunohistochemistry in mSTZ diabetic mice (Fig. 4f). These identified targets can potentially serve as (bio)markers for dysfunctional β-cells, and have the potential to be part of druggable pathways to

restore β-cell function. Some of these were recently also identified in β-cells and pancreata of T1D and T2D human specimens[42,43] (Extended Data Fig. 7g, h). There is a debate to weather β-cell dedifferentiation resembles reversal to a pluripotent (Oct3/4, Nanog, Sox2) or endocrine progenitor state (Ngn3), or is part of normal phenotypic variation described as β-cell heterogeneity, or resembles a glucotoxic-induced reversible state[44]. While dedifferentiated β-cells had been characterized by an upregulation of pluripotency or endocrine TFs[11,12,19], expression levels of *Sox9*, *Pou5f1* (*Oct3/4*), *Myc*, and *Ngn3* were unaltered in mSTZ-treated β-cells (Extended Data Fig. 7i).

To further characterize the transcriptomic state of mSTZ-derived β-cells, we compared our data set to β-cell expression profiles during embryonic (E) 17.5 to postnatal development (P60)[45]. We assessed transcriptional similarity of β-cell subpopulations using Partition-based graph abstraction (PAGA) after data integration and computation of a common embedding. PAGA uses a statistical model to measure the relatedness of groups of single cells[46] (M&M). We found that dedifferentiated β-mSTZ cells were more strongly connected to early time points of the maturation data set, while β2 cells cluster to intermediate time points and β1 cells to late time points (Fig. 5a). Remarkably, the inferred cellular trajectory from β-mSTZ to β2 to β1 cells aligns with the trajectory of β-cell maturation from embryonic (E17.5) to mature β-cells (P60) of the reference data set (Fig. 5b). An increase of known β-cell maturation and a decrease of immaturity markers along this trajectory further indicated that the cells follow a similar (de-)differentiation program (Fig. 5c, d). To validate these findings, we scored each β-cell using the gene sets characteristic for the start (E17.5/P0) and end (P60) point of the developmental trajectory, respectively (Supplemental Table 4 and M&M). Healthy mature β-cells (β1) scored high for maturity genes, while healthy immature cells (β2) and dedifferentiated cells (β-mSTZ) scored higher for the embryonic/immaturity gene set (Fig. 5e). Altogether, this implies that during the transition from healthy β1 to β2 to dedifferentiated β-mSTZ, β-cells revert, at least in part, back to a more immature and further to an embryonic-like state.

To separate the altered maturation state from other processes induced in dedifferentiated β-cells, we compared differentially regulated gene ontologies and pathways between embryonic (E17.5/P0) and mature (P60) β-cells and between mSTZ and healthy control β-cells (M&M). According to the trajectory and PAGA analysis, these β-cell states of the reference data set correspond best to dedifferentiated

mSTZ and mature, healthy β-cells, respectively. Embryonic and mSTZ-diabetic β-cells shared downregulation of molecular processes connected to β-cell function and maturity (e.g. insulin secretion, FoxO signaling) (Extended Data Fig. 8a and Supplemental Table 4), while genes involved in oxidative phosphorylation and gene and protein transcription were upregulated (Extended Data Fig. 8b and Supplemental Table 4). Specific to embryonic β-cells was a downregulation of lipid and carbohydrate metabolism and an upregulation of WNT signaling (Extended Data Fig. 8a, b). This corresponds to known mechanisms of β-cell maturation during embryogenesis[45]. Interestingly, in mSTZ-diabetic β-cells, but not the embryonic β-cells, we found an upregulation of pathways and ontologies associated to ER stress and a decreased expression of genes involved in insulin and MAPK signaling (Extended Data Fig. 8a, b).

Thus, β-cell dedifferentiation involves partial reversal to an embryonic/immature β-cell program and upregulation of an ER stress response and altered signaling state. These results suggest that surviving β-cells are dedifferentiated, which shows that mSTZ-induced diabetes is a good model to study mechanisms of β-cell de- and redifferentiation in the absence of genetic lesions.

Mechanisms of β-cell redifferentiation

In line with the pharmacological data, single cell analysis of the different treatments revealed that β-cells of vehicle (Extended Data Fig. 9a), estrogen (Extended Data Fig. 9b), and GLP-1 (Extended Data Fig. 9c) treated mice remained dedifferentiated. In contrast, we observed an increased fraction of immature β2-cells from GLP-1/estrogen treated mice (Extended Data Fig. 9d). In PEG-insulin (Extended Data Fig. 9e) and GLP-1/estrogen plus PEG-insulin co-treated mice (Extended Data Fig. 9f), almost no dedifferentiated β-cells remained and most cells clustered with immature β2-cells. To further assess the transcriptional state of β-cells from the treated mice, we calculated a cell-to-cell distance so that cells can be ordered along the cellular trajectory from dedifferentiated to healthy β-cells (M&M). On this one-dimensional axis, β-cells of mice treated with PEG-insulin or the combination of PEG-insulin and GLP-1/estrogen were located closest to β-cells from healthy mice (Fig. 6a-c). This transcriptional similarity to healthy β-cells was further supported by PAGA (M&M). In the PAGA graph, β-cells of PEG-insulin and co-treated mice showed the strongest connection to healthy β-cells

(Fig. 6d). The observed overall re-establishment of the healthy β-cell expression profiles was substantiated by an increased expression of β-cell maturity markers and decreased expression of immaturity and dedifferentiation markers along the inferred trajectory (Fig. 6e, f, g). Moreover, Ucn3 expression recovered during the pharmacological treatment (Extended Data Fig. 10). This shows that the maturation state before treatment was different to that achieved after treatment. Hence, upon PEG-insulin or PEG-insulin plus GLP-1/estrogen treatment, β-cells adopt a molecular immature yet functional phenotype that is sufficient for blood glucose normalization and diabetes remission.

β-cells from mice treated with PEG-insulin or the combination of PEG-insulin and GLP-1/estrogen were grouped in distinct β-cell subpopulations albeit at a similar maturation state (Fig. 6b). This implies a compound-specific mechanism-of-action (MOA) that underlies the recovery of β-cell function. To investigate the distinct MOAs of the different treatments, we identified the β-cell-specific transcriptional signature of treated and mSTZ-derived β-cells (Supplemental Table 5). An increase of β-cell functionality and maturation genes (Fig. 6h) was common to both treatments and thus due to improved blood glucose levels and/or stimulation of shared pathways of insulin and GLP-1/estrogen signaling. GLP-1, estrogen, and insulin receptor activation regulates MAPK and FoxO signaling[47–50], which were both increased after PEG-insulin and GLP-1/estrogen and PEG-insulin co-therapy (Fig. 6h). Although we cannot dissect the signaling contribution of each individual receptor, we think that the polypharmacological approach might potentiate the simultaneous activation of commonly regulated pathways.

Unexpectedly, treatment with PEG-insulin elicited a β-cell specific stimulation of the insulin signaling cascade as well as the recently characterized RNA polymerase II mediated pathway[51] (Fig. 4h). Hence, our data suggest that direct effects of insulin on β-cells contribute to improve β-cell function and recovery, as was proposed for T2D[52,53].

Our goal was to use GLP-1/estrogen to selectively deliver estrogen into β-cells. Consistently, we found a β-cell-specific induction of the ER-associated degradation (ERAD) pathway and tRNA signaling in PEG-insulin and GLP-1/estrogen cotreated mice (Fig. 6h). ERAD mitigates ER stress, which when unresolved, contributes to functional β-cell mass loss in T1D and T2D[54]. Chemical and genetic disturbances of ERAD impair β-cell function[55–58]. We found an increased proinsulin to C-peptide ratio

306 in mSTZ-diabetic mice, which is used as ER-stress surrogate in diabetes (Extended Data Fig. 11a)[59,60].
307 GLP-1/estrogen, PEG-insulin, and GLP-1/estrogen and PEG-insulin co-therapy normalized this ratio
308 (Extended Data Fig. 11a). Recently, it has been reported that estrogen via nuclear estrogen receptor
309 alpha signaling stabilizes ERAD-proteins Sel1l and Hrd1in β-cells, which was associated with diabetes
310 amelioration in Akita mice[61]. We found increased co-staining for insulin and Sel1l in GLP-1/estrogen
311 and PEG-insulin co-treated islets already 25 days after treatment initiation (Extended Data Fig. 11b).
312 Beside *Sel1l* and *Hrd1* (Syvn1) upregulation, ERAD-associated gene expression (e.g. *Sdf2l1*, *Herpud1*,
313 *Dnajb11*, *Dnajb9*, *Derl3*, and *Hspa5*) was specifically increased in β-cells of GLP-1/estrogen and PEG-
314 insulin co-treated mice (Extended Data Fig. 11c). Sdf2l1, Herpud1, and Hspa5 encode ERAD-proteins
315 with β-cell beneficial effects that allow proper insulin folding and/or function[62–66]. Dnajb9/11 are
316 chaperones that might aid correct insulin protein folding. Derl3 is required for ER-associated
317 degradation[67]. A specific role in β-cells is unknown, but interestingly, Derl3 expression was shown to
318 protect cardiomyocytes against ER-stress induced death by enhancing ERAD[68]. These results support a
319 role for ERAD activation by GLP-1/estrogen and PEG-insulin co-treatment that induces a treatment
320 specific molecular profile for the protection and regeneration of β-cells (Fig. 6b).
321 Likewise, tRNA signaling is a described intracellular target of estrogen and an increased abundance of
322 tRNA has been associated with proliferating cells[69,70]. Indeed, from the single cell data, we found the
323 highest fraction of proliferative β-cells in the PEG-insulin and GLP-1/estrogen conjugate co-treated
324 mice (Fig. 7a). Moreover, we found increased β-cell proliferation in GLP-1/estrogen and PEG-insulin
325 co-treated mice that was already evident after 25 days of treatment, which importantly was not evident
326 in the single-treatment groups (Fig. 7b). Stressed β-cells, such as under chronic hyperglycemic
327 condition, lack an adequate response to GLP-1 therapy probably due to decreased expression of the
328 GLP-1R[71–74]. Here, we hypothesized that restoring glycemia in mSTZ mice, notably through additional
329 chronic insulin therapy, increased the expression of GLP-1R. Indeed, we found progressively increased
330 levels of GLP-1R on β-cells of mice with improved glucose levels (Fig. 7c). This potentially facilitated
331 the enhanced delivery, uptake and action of estrogen and GLP-1 in β-cells, especially for the co-
332 treatment of GLP-1/estrogen with insulin.

To examine whether other endocrine cells have contributed to the regeneration of functional β-cells, we explored cluster relations and possible cellular transitions using PAGA and RNA velocity estimation (M&M). For this we included mSTZ as the origin (starting point) of treated cells and investigated where cells move from that baseline (Fig. 8a). We found no direct connection or cell movement from other (non-β) cell populations towards redifferentiated β-cells. We next examined the RNA velocity of treated endocrine cells and their potential fate (Fig. 8b). Some of the immature β-cells observed following GLP-1/estrogen, PEG-insulin and their combined treatment pointed towards mature β-cells of healthy mice, thus further substantiating β-cell redifferentiation. Moreover, the scRNA-seq did not suggest increased neogenesis after 100 days of treatment as indicated by unchanged expression levels of *Ngn3* mRNA in endocrine subtypes (Fig. 8c). We also found no indication of overt neogenesis contributing to β-cell regeneration by Ngn3 immunostaining in tissue sections of earlier time points (Fig. 8d). Together, these results suggest redifferentiation of β-cells along de- and redifferentiation trajectories as the main mechanism underlying the re-establishment of functional β-cells in the mSTZ model by GLP-1/estrogen, PEG-insulin, and their co-treatment. By combining low dose insulin with GLP-1/estrogen treatment, we furthermore trigger a β-cell specific transcriptional response characterized by increased β-cell proliferation and enhanced functionality.

Discussion

Herein we have established the mSTZ model of diabetes as model to study β-cell dysfunction and dedifferentiation. Single cell profiling of remaining β-cells discovered many novel markers of β-cell dedifferentiation that code for surface molecules, receptors and secreted proteins. These might be used as biomarkers or allow the detection, isolation and characterization of dedifferentiated β-cells. This could reveal pathomechanisms of T1D and T2D and potentially identify unique diagnostic markers and therapeutic targets. Using scRNA-seq we were able to delineate a β-cell fate trajectory where cells transitioned from mature to immature to dedifferentiated β-cells, implicating that β-cells can be characterized by a continuum of transcriptional states that reflect discrete phenotypes. Inference of cell transitions using the RNA velocity concept further suggested that there was no on-going transdifferentiation from other non-β and non-endocrine cells towards dedifferentiated β-cells.

Upregulation of the endocrine master regulator Ngn3 might depend on severity of hyperglycemia: high glucose levels (> 33mM) were shown to induce Ngn3 expression[12,19], whereas lower levels (< 25mM) were not[18,75,76] (also this study). We show that β-cell dedifferentiation in mSTZ-diabetic mice was independent of an induction of $Ngn3^{+}$ endocrine progenitors and the transcriptional state of dedifferentiated β-cells was more similar to late embryonic or early postnatal β-cells.

Recently, the Kushner laboratory has provided evidence that some of the remaining insulin in the blood stream of long-term T1D patients[77] originates from dedifferentiated β-cells and/or polyhormonal non-β-cells that function as "insulin microsecretors"[78]. Similarly, the Korsgren laboratory found histological evidence for β-cell dedifferentiation at T1D onset[79]. Thus, triggering redifferentiation of dedifferentiation β-cells seems an intuitive approach for the treatment of diabetes, which does not involve β-cell proliferation or neogenesis *per se*[80]. Preclinical as well as clinical findings from type 1 and 2 diabetic patients suggest a transient recovery of β-cell dysfunction upon glycemia normalization by intensive insulin treatment either by β-cell rest or redifferentiation[3,4,19]. By scRNA-seq we can dissect endocrine subtype-specific treatment responses and show that insulin treatment triggers transcriptional changes in β-cells, which are connected to insulin and/or IRS signaling. This supports the idea that besides lowering the glucotoxic stress on β-cells, direct insulin/IGF signaling improves β-cell health and performance and can redifferentiate β-cell mass in diabetic models[53]. Importantly, the redifferentiated β-cells induced by insulin therapy were functional and responded to physiological stimuli as indicated by increased plasma C-peptide levels.

Moreover, we show that targeted delivery of estrogen via GLP-1 as peptide carrier and intensive insulin co-therapy by a distinct MOA alleviates hyperglycemia, increases fasting C-peptide levels and redifferentiates β-cells, while reducing daily insulin requirements by 60% and limiting weight gain of mice. The enhanced restoration of GLP-1R expression in dedifferentiated β-cells by the GLP-1/estrogen and insulin co-treatment renders them susceptible to targeted delivery of estrogen. As previously proposed in the Akita mouse model[61], we observed that stimulating the ERAD pathway by GLP-1/estrogen beneficially influences β-cell physiology in rodent models of diabetes. Finan et al. previously showed that the peptide-based targeting prevented adverse side effects of estrogen, such as uterus and tumor growth[25]. There was also no measurable estrogen-induced increase in bone content due to lack of

or limited GLP-1R expression on off-target tissues and cells[25]. Here, we extended the safety profile and demonstrated that GLP-1/estrogen did not stimulate uterus tissue growth in OVX rats. This study further verified that there is insufficient free, systemic estrogen to drive toxicity as well as the selectivity and specificity of GLP-1–mediated estrogen targeting. The strategy to use GLP-1 as a carrier may be adopted to selectively target any other small molecule or biologic to β-cells. The prerequisite for the transport of the molecule of interest into the target cell, i.e. stressed and dedifferentiated β-cells, is adequate GLP-1R expression. Under hyperglycemic conditions, adjunctive treatments that reduce the glycemic burden, such as chronic insulin therapy as demonstrated here, can facilitate the restoration of GLP-1R expression in stressed β-cells[71,74]. Notably, chronic PEG-insulin treatment also increased functional β-cell number and the scRNA-seq data suggest a direct effect of insulin on β-cells. Thus, combinatorial pharmacological treatments that include insulin might have additional beneficial effects on β-cell survival, protection, proliferation and function. Altogether, our work has identified mechanisms and pathways of β-cell dedifferentiation and opens new avenues for pharmacological targeting these dedifferentiated cells for diabetes remission.

Materials and Methods

STZ treatment. STZ (Sigma-Aldrich Cat, S0130) was injected intraperitoneally in 8-week old male C57BLJ/6 mice (n=125) at 50 mg/kg for five consecutive days following the mSTZ model to induce diabetes. A subset of age-matched male mice was injected with ice-cold citrate buffer (pH 4.5) as control animals (n=20). Ten days after the last STZ injection, fasting blood glucose was taken as well as plasma to determine fasting insulin and C-peptide levels. We included hyperglycemic mice with fasting blood glucose levels > 190 mg/dl (n=116). We estimated β-cell function and mass of STZ treated mice by combining fasting blood glucose levels, the HOMA-β-score, and the ratio of fasting C-peptide to blood glucose levels. Among STZ treated mice, animals with fasting glucose levels > 25^{th} percentile, a HOMA-β-score < 25^{th} percentile, and a C-peptide/blood glucose ratio < 25^{th} percentile were excluded from the study (n=9).

Pharmacological study in mSTZ mice. STZ diabetic mice were randomized and evenly distributed to different treatments according to fasting blood glucose levels. Ten days after the last STZ injection, mice were allocated to different treatments, which were daily subcutaneous injected with vehicle (PBS; n = 17, not STZ-treated), vehicle (PBS; n = 17, STZ-treated), a GLP-1 analog (n = 16), estrogen (n = 14), GLP-1/estrogen (n = 28, of which n = 11 mice were switched to vehicle (PBS) treatment after 12 weeks of GLP-1/estrogen treatment), PEG-insulin (n = 13), or GLP-1/estrogen and PEG-insulin (n = 16) at the indicated doses for 100 days. Mice were housed up to four per cage on a 12:12-h light-dark cycle at 22°C with free access to normal chow diet (Altromin, 1314) and water. Compounds were administered in a vehicle of PBS (Gibco) and were given by daily subcutaneous injections at the indicated doses at a volume of 5 µl per g body weight for the indicated durations. The investigators were not blinded to group allocation during the *in vivo* experiments or to the assessment of longitudinal endpoints. All rodent studies were approved by and performed according to the guidelines of by the Animal Use and Care Committee of Bavaria, Germany.

Study in FVFPBF^{DHOM} mice. 8-week old male FVFPBF^{DHOM} mice with fasting blood glucose > 250 mg/dl were randomized to vehicle (n = 7), estrogen (n = 5), GLP-1 (n = 9), or GLP-1/estrogen (n = 11)

treatment according to their fasting blood glucose levels. Mice were treated daily for four weeks with subcutaneous injections. Fasting blood glucose was measured after a 6h-fast. We single- or group-housed the mice on a 12-h light, 12-h dark cycle at 22 °C with free access to food and water. This study were approved by and performed according to the guidelines of by the Animal Use and Care Committee of Bavaria, Germany.

Uterotrophic Assessment in Ovariectomized Rats. The study was designed in accordance with the Endocrine Disruptor Screening Program Test Guidelines OPPTS 890.1600: Uterotrophic Assay, a standardized *in vivo* screening test intended to evaluate the ability of a chemical to elicit biological activities consistent with agonists of natural estrogens (e.g., 17ß-estradiol). It is based on the increase in uterine weight or uterotrophic response The study was further designed according to accepted pharmacological principles and followed Good Laboratory Practice (conducted by Envigo CRS Limited, UK). A total of 44 ovariectomized female Sprague-Dawley rats (Charles River UK, Ltd) were supplied for the study, of which 40 animals were allocated to treatment groups (randomized by body weight to ensure equal group mean starting body weight) and the remaining 4 animals were allocated as spares. On the day of dosing (following 14-22 days of acclimatization), rats were approximately 9-12 weeks of age, and weighed 217 g to 348 g. Four groups of 8 rats each were treated for 14 consecutive days with once-daily subcutaneous administration of GLP-1/estrogen at doses of 400, 2200 and 4000 µg/kg/day or volume-matched vehicle (PBS). An additional group of animals received once-daily subcutaneous injections of vehicle for the first 10 days followed by once-daily subcutaneous injection of 17 alpha-ethynyl estradiol (positive control) at 300 µg/kg/day on Days 11 to 14. Animals were weighed daily from Day 1 (prior to dosing) until the day of necropsy, and food consumption recorded on Days -4, 1, 4, 8, 11, and 15 (day of necropsy). Standard toxicological organ weight measurement was carried out at necropsy, including the weighing of wet and dry (blotted) uterine tissue. The uterus was sampled and weighed according to OPPTS 890.1600.

Administration of EdU. To investigate cell proliferation, we used the modified Uracil analog 5´ethynyl-2´-desoxyuridine (EdU). 50µg/Kg body weight of EdU was injected intraperitoneal (i.p.) 36 and 24 hrs prior to their sacrifice.

Compound formulations. The synthesis, purification, and characterization of GLP-1 and the GLP-1/estrogen co-agonist was described previously[25] and was used without any further chemical modification or change in formulation. Pegylated insulin (PEG-insulin) was prepared by the insulin N-terminal amine reductive amination with 20K Methoxy PEG Propionaldehyde. Briefly, human insulin was dissolved in 50mM Sodium Acetate buffer (pH 5.0) and 50% acetonitrile. A 30-fold excess of sodium cyanoborohydride and a 1.5-fold excess of methoxy PEG propionaldehyde (M-ALD-20K, JenKem Technology USA Inc., Plano, TX) was added to the buffer containing insulin for 3h at room temperature with stirring. Purification by reverse phase chromatography on a C-8 column in 0.1%TFA acetonitrile solvents yielded the final product at greater than 95% purity. Estrogen (17β-Estradiol, Sigma) was dissolved in 100% ethanol (Sigma) at a concentration of 1 mg/ml and diluted with PBS to the needed concentration.

Blood parameters. Blood was collected from tail veins after a 4-hour fast, using EDTA-coated microvette tubes (Sarstedt). Blood was immediately chilled on ice. Plasma was separated by centrifugation at 5000 g at 4 °C for 10 min using a micro centrifuge and stored at -20°C until further usage. Plasma insulin and C-peptide (Crystal Chem) and Proinsulin (Alpco) were quantified by enzyme linked immunosorbent assays following the manufactures' instructions. 4-h fasting blood glucose levels were determined using a handheld glucometer (FreeStyle).

Pancreas Dissection. Adult pancreata were dissected and fixed in 4% PFA in PBS for 24 hrs at 4 °C. The tissues were cryoprotected in a sequential gradient of 7.5, 15 and 30% sucrose-PBS solutions at RT (2h incubation for each solution). Next, the pancreas were incubated in 30% sucrose and tissue embedding medium (Leica) (1:1) at 4 ºC overnight (O/N). Afterwards, they were embedded in cryoblock using tissue-freezing medium (Leica), frozen in dry ice and stored at -80º C. Sections of 20 µm thickness

were cut from each sample mounted on a glass slide (Thermo Fisher Scientific) and dried for 10 min at RT before use or storage at -20 °C.

Sections Immunostainings. The cryosections were rehydrated by 3x washing with 1X PBS, permeabilized with 0.2-0.15% Triton X-100 in H_2O for 30 min. Permeabilization was not performed for stainings with GLP-1R. Then, the samples were blocked in blocking solution (PBS, 0.1% Tween-20, 1% donkey serum, 5% FCS) during 1 hour. The following primary antibodies were used: guinea pig polyclonal anti-insulin (1:300, Thermo Scientific), goat polyclonal anti-Glut2 (1:500, Abcam), goat polyclonal anti-Nkx6.1 (1:200, R&D systems), goat polyclonal anti-somatostatin (1:500, Santa Cruz), rat monoclonal anti-somatostatin (1:300, Invitrogen), rabbit polyclonal anti-urocortin 3 (1:300, Phoenix Pharmaceuticals), rabbit monoclonal anti-insulin (1:300, Cell Signaling), guinea pig polyclonal anti-glucagon (1:500, Takara), guinea pig polyclonal anti-insulin (1:300, ABD Serotec), rabbit polyclonal cleaved caspase-3 (Asp 175) (1:300, Cell Signaling), rabbit monoclonal anti-ki67 (1:300, Abcam), rabbit polyclonal anti-Aldh1a3 (1:300, Abcam), rabbit monoclonal anti-GLP-1R (1 µg/ml, Novo Nordisk), rabbit polyclonal anti-gastrin (1:100, Abcam), rabbit polyclonal anti-cholecystokinin (1:100, ENZO life sciences), goat polyclonal anti-Sel1l (1:300, Novus Biologicals), and rabbit anti-Ngn3 (1:800, donated by H. Edlund). Dilutions were prepared in blocking solution and sections were incubated O/N at 4°C. Thereafter, sections were rinsed 3x and washed 3x with 1X PBS. All secondary antibodies were used at a 1:800 dilution prepared in blocking buffer. We used the following secondary antibodies: donkey anti-Goat IgG (H+L) secondary antibody (Alexa Fluor 633 Invitrogen A-2108), donkey anti-Rabbit IgG (H+L) secondary antibody (Alexa Fluor 555 Invitrogen A-31572); donkey anti-Rabbit IgG (H+L) secondary antibody (Alexa Fluor 488 Invitrogen A-21206); donkey anti-Guinea pig IgG (H+L) secondary antibody (DyLight 649 Dianova 706-495-148); donkey anti-Rat IgG (H+L) secondary antibody (DyLight 647 Dianova 711-605-152); donkey anti-Rat IgG (H+L) secondary antibody (Cy3 Dianova 712-165-153); donkey anti-Guinea pig (H+L) secondary antibody (Alexa Fluor 488 Dianova 706-545-148). After 4-5h of incubation, pancreatic sections were stained with DAPI (1:500 in 1X PBS) for 30 min, rinsed and washed 3x with 1X PBS and subsequently mounted. All images were

obtained with a Leica microscope of the type DMI 6000 using the LAS AF software. Images were analyzed using the LAS AF and/or ImageJ software program.

Automatic tissue analysis. Stained tissue sections were scanned with an AxioScan. Z1 digital slide scanner (Zeiss, Jena, Germany) equipped with a 20X magnification objective. We scanned 3 sections per animal. Images were evaluated using the commercially available image analysis software Definiens Developer XD 2 (Definiens AG, Munich, Germany) following a previously published procedure (Feuchtinger et al., 2014). In a first step regions of interest were annotated manually in order to select islets of Langerhans for analysis. A specific rule set was then defined to detect and quantify the cells within each defined region, based on the fluorescence intensity of DAPI, morphology, size and neighborhood. The insulin, glucagon, or somatostatin expressing cells were classified automatically using the fluorescence intensity of each hormone.

EdU detection protocol. EdU staining was carried out according to the EdU imaging kit manual (Life Technologies) after staining with the 2nd antibody. DAPI staining and mounting was performed as mentioned above.

Pancreatic insulin content. Pancreatic insulin content was determined by an acid ethanol extraction. The pancreas was dissected, washed (1X PBS) and homogenized in an acid-ethanol solution (5mL 1.5% HCl in 70% EtOH) followed by incubation at -20°C for 24h. After 2 rounds of acid-ethanol precipitation, the tissue was centrifuged (2000 rpm, 15 min, 4°C) and the supernatant neutralized with 1M Tris pH 7.5. Insulin was measured using a mouse insulin ELISA (Crystal Chem) and normalized over the protein concentration that was determined by BCA protein assay.

Islet isolation. Islet isolation was performed by collagenase P (Roche) digestion of the adult pancreas. Briefly, 3 mL of collagenase P (1 mg/mL) was injected into the bile duct and the perfused pancreas was consequently dissected and placed into another 3 mL collagenase P for 15 min at 37 °C. 10 mL of G-solution (HBSS (Lonza) + 1% BSA (Sigma)) was added to the samples followed by centrifugation at 1600 rpm at 4 °C. After another washing step with G-solution, the pellets were re-suspended in 5.5 mL of gradient preparation (5 mL 10% RPMI (Lonza) + 3 mL 40% Optiprep (Sigma)/ per sample), and

placed on top of 2.5 mL of the same solution. To form a 3-layers gradient, 6 mL of G-solution was added on the top. Samples were then incubated for 10 min at RT before subjecting to centrifugation at 1700 rpm. Finally, the interphase between the upper and the middle layers of the gradient was harvested and filtered through a 70 μm Nylon filter and washed with G-solution. Islets were handpicked under the microscope.

Single cell suspension. In order to achieve a single cell suspension of islets, islets were handpicked in an 1.5 mL Eppendorf tube, pelleted (800 rpm, 1 min) washed with PBS (-Mg/Ca, Gibco) and digested with 0.25% Trypsin with EDTA (Gibco) at 37°C for 8 min. Mechanical disaggregation every 2-3 min was required. After, the digestive reaction was stopped and cells were pelleted (1200 rpm, 5 min).

Single cell sequencing. Single cell libraries were generated using the Chromium™ Single cell 3`library and gel bead kit v2 (PN #120237) from 10x Genomics. Briefly, to reach a target cell number of 10.000 cells per sample 16.000 cells per sample were loaded onto a channel of the 10X chip to produce Gel Bead-in-Emulsions (GEMs). This underwent reverse transcription to barcode RNA before cleanup and cDNA amplification followed by enzymatic fragmentation and 5´adaptor and sample index attachment. Libraries were sequenced on the HiSeq4000 (Illumina) with 150bp paired-end sequencing of read2.

FACS sorting. FACS sorting of endocrine cells was perfomerd using the FACS-Aria III (BD). Single cells were gated according to their FSC-A (front scatter area) and SSC-A (side scatter area). Singlets were gated dependent on the FSC-W (front scatter width) and FSC-H (front scatter height) and dead cells were excluded using the marker 7AAD (eBioscience). The FVF endocrine populations were discriminated upon their Venus fluorescence emission at 488 nm and the β- and α-lineages according to their BFP emission at 405 nm (positive and negative respectively). To enrich for β-cells the distinct SSC-A high populations were gated. In order to isolate RNA from FACS sorted cells, they were sorted directly into Qiazol (Qiagen).

RNA Isolation and cDNA preparation. The mRNA isolation was performed using the miRNA micro kit (Qiagen) according to the manual. On column DNase I treatment was applied to degrade DNA. For

cDNA preparation the SuperScript Vilo cDNA and cDNA synthesis kit (Life Technologies and Promega respectively) were used. The cDNA synthesis was carried out according to the kit manual.

Quantitative PCR (qPCR). The qPCR was carried out using Viia7 Real Time PCR System (Thermo Fisher Scientific) and TaqMan™ probes (Life Technologies): Ins 1 (Mm01950294_s1), Ins 2 (Mm00731595_Gh), Glucagon (Mm01269055_m1), Somatostatin (Mm00436671_m1), Ppy (Mm01250509_g1), Ghrelin (Mm00445450_m1), Pecam1 (Mm01242584_m1), Gapdh (Mm99999915_g1) and 18S (Mm03928990_g1). Each reaction contained 25 ng of cDNA. For analysis, the C_t-values were transformed to the linear expression values and normalized to the reference genes (GAPDH & 18S) and to the control samples.

Reaggregated human micro-islets. All primary human islets were obtained through Prodo Laboratories Inc. Irvine, CA with no information on the identity of the donor for ethical and privacy reasons (donor 1: male, BMI 32.38, age 48, HbA1c 5.6%; donor 2: male, BMI 33.2, age 46, HbA1c 5.4%; donor 3: male, BMI 28.65, age 34, HbA1c 5.2%). For all donors, consent was obtained from next of kin. For each production of InSphero 3D InSight™ human islet microtissues, 10'000 - 20'000 islet equivalents were dispersed in dissociation solution (1X TrypLE™ Express solution - Thermo Fisher Scientific #12604013, with 40 µg/ml DNase I - Sigma-Aldrich #10104159001) by gentle pipetting at 37 °C. Remaining cell clumps were removed by filtering the cell suspension through a cell strainer (70 µm pore size). Islet microtissues were produced by hanging-drop based scaffold-free reaggregation of 2500 cells in each well of the InSphero's 96-well Hanging Drop System for 5 days. The primary aggregates were then transferred to the Akura™ 96 well-plate to further mature for at least another 8 days before the start of the experiments. All experiments were performed within 30 days after the start of the aggregation. Islet microtissues were maintained in 3D InSight™ Human Islet Maintenance Medium (InSphero AG, Schlieren, Switzerland).

Compound, cytokine treatments and GSIS with human micro-islets. Dilution series of compounds were performed in in 3D InSight™ Human Islet Maintenance Medium. Each of the assessed compounds were added to the culture medium at indicated concentration one day prior to the start of the cytokine

582 treatment. The cytokine cocktail containing; tumor necrosis factor alpha (TNFα, 10 ng/mL, Thermo
583 Fisher Scientific #PHC3016), interferon gamma (IFNϒ, 10 ng/mL, Sigma-Aldrich #I3265) and
584 interleukin-1beta (IL-1β, 2 ng/mL, Sigma-Aldrich #I17001), was prepared in PBS containing 0.1%
585 Bovine Serum Albumin (BSA, Sigma-Aldrich #A7888). Same concentration of PBS-BSA solution was
586 maintained in each experimental condition. Regular redosings with cytokines and compounds were
587 performed every 2-3 days. Prior to GSIS, culture medium was removed and islet microtissues were
588 washed twice with Krebs Ringer Hepes Buffer (KRHB – 131 mM NaCl, 4.8 mM KCl, 1.3 mM CaCl2,
589 25 mM Hepes, 1.2 mMm Kh2PO4, 1.2 mM MgSO4, 0.5% BSA) containing 2.8 mM glucose and
590 equilibrated for 1 hour in the same solution. GSIS was performed in KRHB containing indicated glucose
591 concentrations for 2 hours. Following GSIS, the tissues were lysed using CellTiter-Glo® Luminescent
592 Cell Viability Assay (Promega #G9241, with protease inhibitor cocktail, Promega #G6521) and the
593 luminescence was recorded with a microplate reader (Infinite M1000, TECAN, Switzerland) for the
594 analysis of total ATP content. The lysates were then used for assessment of total insulin content. After
595 proper dilutions in KRHB were performed, total and secreted insulin was quantified using Stellux®
596 Chemi Human Insulin ELISA (Alpco, 80-INSHU-CH10). Caspase-Glo® 3/7 Assay (Promega, #G8090)
597 was used on to assess caspase-3/7 activity in the islet microtissues following compound treatment.
598 **Statistical analysis not including scRNA-seq data.** Preliminary data processing and calculations
599 during ongoing studies was done using Microsoft Excel 2016. All further statistical analyses were
600 performed using GraphPad Prism 8. We used the one-way analysis of variances (ANOVA) followed by
601 Tukey's post hoc analysis to determine significance among different treatment groups. In case of only
602 two groups, the unpaired Student two-tailed t-test was used to detect significant differences. The human
603 micro-islets derived from three different donors, which naturally varied in their GSIS. To compare the
604 treatment effects among all donors, we used one-way ANOVA with the different donors as random
605 effect followed by Tukey's post hoc analysis. This analysis was performed in R. A Grubbs test ($\alpha <$
606 0.05) was used to detect significant outliers, which were then excluded from subsequent statistical

analysis and figure drawing. $P < 0.05$ was considered statistically significant. All results are mean ± SEM unless otherwise indicated.

Preprocessing of droplet-based scRNA-seq data. Demultiplexing of raw base call (BCL) files, alignment, read filtering, barcode and UMI counting were performed using the CellRanger analysis pipeline (Version 2.0.0) provided by 10X Genomics. High quality barcodes were selected based on the overall distribution of total UMI counts per cell using the standard CellRanger cell detection algorithm. All further analyses were run with python3 using the scanpy package[81] (v1.0.4+92.g9a754bb, https://github.com/theislab/scanpy) except stated otherwise. Genes with expression in less than 10 cells were excluded. Further, as also applied as standard preprocessing steps in scanpy tutorials, low quality or outlier cells were removed if they (i) had a high fraction of counts from mitochondrial genes (40% or more), (ii) expressed more than 7000 genes, or (iii) had more than 100'000 UMI counts. Cell by gene count matrices of all samples were then concatenated to a single matrix. To account for differences in sequencing depth, UMI counts of each cell were normalized by total counts of that cell (pp.normalize_per_cell with mean=TRUE) and values log-transformed. 1625 highly variable genes were selected based on normalized dispersion using the setting the lower cutoffs for the mean to 0.0125 and for the dispersion to 0.5. This matrix was used as input for all further analyses unless stated differently.

Embedding, clustering and cell type annotation. Clustering was performed on the full data set to reduce systematic biases such as batch effects as recently recommended[82]. A single cell neighborhood graph (kNN-graph) was computed on the 50 first principal components using 15 neighbors. To minimize condition effects and facilitate clustering we recomputed the kNN-graph using the first 15 diffusion components of the PCA-based graph as suggested[46]. For clustering and cell type annotation, louvain-based clustering[83] was used as implemented in louvain-igraph (v0.6.1 https://github.com/vtraag/louvain-igraph) and adopted by scanpy (tl.louvain). The resolution parameter was varied in different parts of the data manifold to account for strong changes in resolution (for details see available code). Clusters were annotated based on the mRNA expression of the four main hormones *Ins1* and *Ins2*, *Gcg*, *Sst* and *Ppy*

633 (endocrine cells) and other known marker genes (non-endocrine cells) and were merged if only
634 reflecting heterogeneity within a cell type not in the focus of this study.
635 Ductal cells (expressing *Krt19*), acinar cells (expressing *Prss2*), endothelial cells (expressing *Plvap*),
636 stellate cells (expressing *Col1a2*) and small clusters of potential doublet-like cells co-expressing
637 endocrine and non-endocrine markers were removed from further analysis. Immune cells (expressing
638 *Cd74*) infiltrating the islets were finely subclustered into Macrophages (expressing *Cd86*, *Adgre1* and
639 *Cd14*), Dendritic cells (expressing *Cd86*, *Itgax* and *Iftim3*), B cells (expressing *Cd79a* and *Cd79b*) and
640 T cells (expressing *Cd8a* and *Cd3d*).
641 The hormones *Ins1* and *Ins2*, *Gcg*, *Sst* and *Ppy* were expressed at very high levels and showed
642 background level expression in all other endocrine subtypes and non-endocrine cell types. Such
643 background expression is a common phenomenon in droplet-based scRNAseq data. It is commonly said
644 to be due to free-floating mRNA in the single-cell solution that comes from lysed cells and that is
645 incorporated into all droplets. For annotation, only hormone expression that was well above the
646 background level in non-endocrine cells such as ductal, immune and endothelial cells was considered.
647 For the identification of β-cell substates a new kNN-graph on the first 50 principal components was
648 calculated and put into louvain-based clustering of both Ins monohormonal and the connected Ins-PP
649 cells. Similarly, Ins-Sst cells were subclustered from Ins-Sst-PP cells after recalculating the kNN-graph
650 on the first 50 principal components. Ins-Gcg-Sst cells were assigned using a manual threshold for all
651 three hormones that was well above ambient levels (threshold = 6 for normalized data).
652 For visualization, Uniform Manifold Approximation and Projection (UMAP) was run as recently
653 recommended[84]. For each UMAP-plot the UMAP was newly calculated by recomputing the kNN-graph
654 on the represented cell subset using the first 50 principal components.
655 **Identification of polyhormonal singlets and doublet-like endocrine cell clusters.** Polyhormonal cells
656 have previously been described to exist in pancreatic islets[85–87]. Still, the expression of multiple
657 hormones in the same droplet can also be an indication for a doublet. It can therefore be difficult to
658 distinguish polyhormonal singlets from doublets. A doublet rate of approx. 8-10% was measured in

experiments with the same concentration of cells using the 10X technology[88]. This rate includes doublets with contributions from two different cell types (here polyhormonal doublets) and from the same cell type (here monohormonal doublets). The latter type of doublets resemble monohormonal singlets and do not affect subsequent analyses[89]. We calculated the expected doublet frequency of polyhormonal doublets for a doublet rate of 10% using the frequency of monohormonal cell types that contribute to the doublet (doublet contributors) and assuming that doublets are generated by sampling singlet cells uniformly at random[89]. In every sample the proportion of observed polyhormonal cells clearly exceeded the expected polyhormonal doublet frequency. Thus, in our data set it is unlikely that all detected polyhormonal cells are doublets. Application of doublet cell detection tools Scrublet[89] (v0.1, https://github.com/AllonKleinLab/scrublet) and DoubletDetection (https://github.com/JonathanShor/DoubletDetection) failed to resolve which clusters represent doublets and which represent polyhormonal singlets. Predictions of the tools disagreed and the doublet rate was consistently overestimated. We therefore used the following criteria to evaluate polyhormonal cell clusters and distinguish between singlets and doublets:

(i) Doublets should not express unique genes. All genes should also be expressed in at least one doublet contributor.

(ii) Doublets should express marker genes or lineage-determining transcription factors of the doublet contributors. Downregulation of these genes indicate singlet populations.

(iii) Previous reporting of polyhormonal singlet cells in literature.

(iv) Clusters of polyhormonal cells with higher frequency than expected by our doublet simulation indicate polyhormonal singlet clusters (Extended Data Fig. 6g).

(v) Clusters with Scrublet doublet score distribution that are comparable to monohormonal singlet clusters indicate polyhormonal singlets (Extended Data Fig. 6h).

Based on these criteria we found sufficient evidence for Ins-PP, Ins-Sst-PP, Gcg-PP (low) and Gcg-PP (high) cells to be polyhormonal singlets, but excluded Ins-PP-Gcg, Ins-Gcg, Ins-Gcg-Sst, Gcg-Sst-PP and Sst-PP(high) cells as likely doublets.

685 **Cell cycle classification.** To classify cells into cycling and non-cycling cells, first, a score was assigned
686 to each cell for a set of S and G2/M phase genes[90] as proposed[91], and, second, all cells with a S-score or
687 a G2/M-score > 0.25 were classified as cycling. The threshold was chosen based on the score
688 distribution. The score for a given gene set was computed as described[92] and implemented in scanpy
689 (tl.score_genes_cell_cycle).
690 **Marker genes of main endocrine cell types.** For the characterization of the four endocrine cell types,
691 specific marker genes were identified by comparing the gene expression profile of each cell type against
692 all cells of the other three cell types using a the test with overestimated variance as implemented in
693 scanpy (tl.rank_genes_groups). As marker genes, all genes were considered that ranked within the top
694 300 genes, had a test score >8 and were unique markers for one cell type.
695 **Differential expression testing to describe subpopulations and treatment responses.** Differential
696 expression testing between treatments and for the characterization of immature β-cells and
697 polyhormonal subpopulations was performed on quantile-normalized (quantile threshold=0.95) and log-
698 transformed data to account for extremely high expressed genes (e.g. the main hormones in endocrine
699 cells) that may wrongly alleviate the expression of other genes in a cell when applying total count
700 normalization. By quantile normalization each cell is normalized by the total UMI count in the cell of
701 genes that account for less than 5% of the total UMI counts across all cells. Thus, very highly expressed
702 genes are not considered for normalization. For differential expression testing limma-trend[93,94] as
703 implemented in the Bioconductor package limma (v3.28.10) via an rpy2 (v2.9.1) interface was used, as
704 recommended by Soneson and Robinson[95]. In each test only genes expressed in > 1% of cells in any of
705 the two subsets tested were considered. Gene set enrichment was performed using EnrichR[96] via its web
706 interface. As input genes with a FDR < 0.01 and an estimated logFC (output from limma model not the
707 actual logFC as log-transformed data was the input) > 0.25 were used. Of note, the hormones *Ins1* and
708 *Ins2*, *Gcg*, *Sst* and *Ppy* as well as other known cell type marker genes (*Pyy, Iapp, Ttr, Gpx3, Ctrb1,*
709 *Try5)* were differentially expressed also in other cell-types in which they are only expressed at

background levels (free-floating mRNA, see section Embedding, Clustering and annotation). These genes were indicated in Supplemental Tables and excluded for plotting.

Identification of specific β-cell dedifferentiation markers. Genes specific for dedifferentiated β-cells (β-STZ) were extracted from the list of all significantly upregulated genes (FDR < 0.05, estimated logFC > 0.25) in β-cells from mSTZ treated mice compared to β-cells of healthy mice by two filtering steps. First, non-specific genes that were also differentially expressed in any of the other monohormonal endocrine cell types (alpha, delta, PP) were excluded. Second, only genes that were expressed in at least 25% of β-cells from mSTZ treated mice and in less than 5% of β-cells of healthy mice were considered. Location was extracted from the GeneCards database (https://www.genecards.org).

Inference of β-cell maturation, dedifferentiation and regeneration trajectories. Pseudotime of β-cell maturation in healthy islets and dedifferentiation upon STZ treatment was calculated using diffusion pseudotime (dpt)[30] as implemented in scanpy (tl.dpt), selecting a random root cell within the starting population. The choice of root cell did not affect the inferred pseudotemporal ordering strongly. Similarly, the dpt approach was used to model β-cell regeneration and estimate the location of treated β-cells along the path from dedifferentiated to mature β-cells. Here, dpt was used as a cell-to-cell distance metric across samples. Cycling cells as well as a small subpopulation of β-cells were excluded for visualization as they were not part of the linear trajectory and showed very high pseudotime values.

Comparison of b-cell dedifferentiation trajectory to embryonic and postnatal maturation. To compare the dedifferentiation trajectory to embryonic and postnatal maturation we used a publicly available single-cell RNAseq data as a reference that contained cells sorted using a Gcg-Venus and Ins-GFP reporter mice at 6 different time points (E17.5, P0, P3, P9, P18, P60)[45]. The filtered and annotated raw count matrix was downloaded from GEO (accession number GEO: GSE87375). The analysis was run using the updated scanpy package v1.4.4 as only this version includes the necessary data integration methods. ERCCs and genes with expression in less than 3 cells were excluded. The data was normalized to total counts per cell using the *pp.normalize_total* function in scanpy with default parameters and excluding highly expressed genes, and log-transformed (*pp.log1p*). For the scope of this manuscript we

used a subset of the data that contained only β-cells (*Ins1*-positive) cells. Therefore, we computed a kNN-graph on the 50 first principal components using 15 neighbors and performed a first round of louvain-based clustering (tl.louvain). As input data was subset to the 3000 top ranking highly variable genes (pp.highly_variable_genes). We excluded all clusters that showed high expression of *Gcg* (alpha cells) or that showed high expression of *Mki67* indicative of proliferative cells. In addition, we filtered cells that showed high expression of the delta cell markers *Sst* or *Hhex.*

To compute a common embedding and trajectory we integrated this reference data set with the data of this study subset to β-cells from Ctrl and STZ-Vehicle treatment using Bbknn[97] from the scanpy external package (sce). To reduce noise, we excluded genes expressed in less than 15 cells in each data set. In addition, cycling cells (*Mki67*>1, 33 cells of the reference cells, 30 cells of the cells from this study) were excluded as cell cycle dominates their expression profile and these cells therefore formed a separate cluster not part of the linear maturation trajectory. To ensure that β-cell maturation dominates the gene expression variation we, first, only considered the 2000 top ranked highly variable genes (pp.highly_variable_genes) of the reference data set that were also expressed in our data, and, second, reduced the contribution of heterogeneity within the β1 and β-mSTZ cluster to gene expression variation by randomly subsetting both clusters to 500 cells. We then scaled and zero centered each data set separately (pp.scale) and concatenated the two data sets which resulted in a 1788 cells by 1654 genes count matrix. We computed a common kNN-graph on the first 10 principal components using the sce.pp.bbknn function with default parameters and k=5 within batch neighbors. As the data sets did not show a strong batch effect even without integration, assessed by visual inspection of the first principal components and diffusion components, and thus transitions between cells from the two data sets also showed a high probability, we were able to use diffusion pseudotime (tl.dpt) to infer the maturation trajectory with the common kNN-graph as input. The trajectory was calculated selecting a random root cell from the embryonic cells sampled at E17.5. The choice of root cell did not affect the inferred ordering strongly. The ordering of the cells from each data set was largely consistent with the ordering obtained prior to integration, assessed by the distribution along the trajectory of the time points or β-cell

762 subgroups, respectively. To quantify cluster similarity, PAGA was applied to the common kNN-graph
763 (tl.paga).
764 To compute an embryonic/neonatal and a maturity cell score we extracted the gene signatures from the
765 reference data set. The reference data was subset to the 2000 top ranked highly variable genes and
766 louvain-based clustering performed on the kNN-graph computed on the first 50 principal components
767 with 15 neighbors. The cluster consisting of cells sampled at E17.5 and P0 was annotated as
768 embryonic/neonatal, while the cluster consisting mainly of cells sampled from P60 was annotated as
769 mature. Differentially expressed genes between these two clusters were used for scoring. Genes
770 upregulated in the mature or embryonic/neonatal cluster were used as a gene set for maturity or
771 embryonic/immaturity score, respectively. For differential expression testing the t-test with
772 overestimated variance implemented in the tl.rank_genes_groups function of scanpy was used. Top 500
773 ranked genes with a log foldchange > 0.25 and an adjusted p-value <0.01 were considered. Cell scores
774 were computed using the tl.score_genes function in scanpy.
775 **Inference of cluster-to-cluster distances, lineage relations and cell movement.** PAGA[46] was
776 performed to infer cluster and lineage relations using the tl.paga function of scanpy with a threshold on
777 edge significance of 0.05. In a PAGA graph, paths represent cluster connections or relations indicating
778 potential routes of cell transitions. Edge weights represent the confidence of a connection calculated
779 based on a measure of cluster connectivity.
780 To infer the direction of possible transitions[98] and cell movements we estimated RNA velocity using a
781 stochastic version implemented in the scVelo python package (v0.1.16.dev13+c1a6dad,
782 https://github.com/theislab/scvelo with scanpy v1.3.2). Splicing information of reads was extracted
783 using the velocyto pipeline (v0.17.7, http://velocyto.org). We then followed the recommended steps
784 described in scVelo to estimate RNA velocities and RNA velocity force fields. First, data was
785 preprocessed by filtering genes with less than 30 spliced or 30 unspliced counts and both unspliced and
786 spliced counts were normalized by total counts. Then the first- and second order-moments for each cell
787 were computed across its 15 nearest neighbors of the kNN graph in PC space (50 PCs). Next, RNA

velocities were estimated using a stochastic model of transcriptional dynamics. To obtain a more conservative estimate a 95% quantile fit was used. Finally, to project the velocity vector of each cell into the low-dimensional UMAP embedding for visualization and interpretation the expected mean direction given all potential cell transitions on the kNN graph is computed. Each potential cell transition is assigned a probability corresponding to the correlation to the predicted transition by the velocity vector (velocity graph). For example, a high probability corresponds to a high correlation with the velocity vector. The projection results in a low dimensional map of RNA velocity indicating the predicted cell state transitions. For computation of the velocity graph and embedding only genes with a $r2 > 0.1$ of the velocity fit were considered.

The velocities of each gene were calculated over all treatments except for healthy β-cells, where only healthy cells were used. A treatment can here be considered as a state where cells move from the diseased cells potentially towards healthy cells as for pseudotime inference described above. During this process genes are induced and or repressed which is approximated by RNA velocity. Thus, to take into account also these intermediate gene states all treatments were included for model fitting and velocity estimation. Both PAGA and the RNA velocity graphand projection were then instead only computed on the represented cell subset. For this, the kNN-graph was recalculated for the cell subset using the first 50 principal components and the highly variable genes as initially defined.

Data and software availability. Custom python scripts written for performing scRNA-seq data analysis will be made available in a github repository upon publication. Versions of packages that might influence numerical results are indicated in the scripts. Raw data and gene expression matrices of scRNA-seq are deposited on GEO under the accession number GSE128565 (password on request).

Author contributions. S.S. performed in vivo and ex vivo rodent experiments, pancreas histology, analyzed and interpreted all data, interpreted scRNA-seq data, and wrote the manuscript. A.B-P. performed ex vivo rodent experiments, pancreas histology, analyzed and interpreted data, and co-wrote the manuscript. S.T. analyzed and interpreted scRNA-seq data and co-wrote the manuscript. M.B. performed ex vivo experiments and helped drafting the manuscript. A.B. performed ex vivo experiments and helped preparing the single cell suspensions for scRNA-seq. M.A.S.-G., K.F., S.J, A.H., and M.K. performed in vivo experiments and helped interpreting data. E.B. and S.R. ex vivo experiments and helped interpreting data. S.U. interpreted data. A.F. conducted and analyzed the automatic pancreatic histology. B.Y. and A.N. perfomed, analyzed, and interpreted human micro-islets experiments and co-wrote the manuscript. C.B.J. designed, analyzed, interpreted and supervised the rat study, interpreted also other in vivo data and helped writing the manuscript. B.Y. synthesized and characterized compounds used for this study. B.F. designed the in vivo rodent experiment, synthesized and characterized compounds, interpreted the data, and helped writing the manuscript. R.D.D. and M.H.T conceptualized and interpreted all studies and helped writing the manuscript. F.T. conceptualized, supervised, and interpreted the scRNAseq analysis and helped writing the manuscript. S.M.H, T.D.M, and H.L. conceptualized, designed, supervised, and interpreted all studies and wrote the manuscript.

Acknowledgements. We thank Luisa Müller, Laura Sehrer, Emiljia Malogajski, and Marlene Kilian from the Helmholtz Diabetes Center in Munich for excellent assistance with in vivo mouse experiments. We thank Jessica Jaki, Ciro Salinno, Francesco Volta, Julia Beckenbauer, Anne Savoca, and Robert Fimmen for excellent assistance with in vitro experiments. We thank Charles Pyke and Pia Gottrup Mortensen for providing the GLP-1R antibody. We thank Volker Bergen, Malte Lücken, Lukas Simon and David Fischer for fruitful discussions on the computational analysis.

Conflicts of interest. C.B.J., M.C., B.Y, B.F., and R.D.D. are current employees of Novo Nordisk. Novo Nordisk has licensed from Indiana University intellectual property pertaining to this report.

References

1. Matveyenko, A. V. & Butler, P. C. Relationship between β-cell mass and diabetes onset. *Diabetes Obes. Metab.* **10**, 23–31 (2008).
2. Herold, K. C. *et al.* An Anti-CD3 Antibody, Teplizumab, in Relatives at Risk for Type 1 Diabetes. *N. Engl. J. Med.* (2019) doi:10.1056/NEJMoa1902226.
3. Harrison, L. B., Adams-Huet, B., Raskin, P. & Lingvay, I. -Cell Function Preservation After 3.5 Years of Intensive Diabetes Therapy. *Diabetes Care* **35**, 1406–1412 (2012).
4. Kramer, C. K., Zinman, B. & Retnakaran, R. Short-term intensive insulin therapy in type 2 diabetes mellitus: a systematic review and meta-analysis. *Lancet Diabetes Endocrinol.* **1**, 28–34 (2013).
5. Chen, H.-S. *et al.* Beneficial Effects of Insulin on Glycemic Control and -Cell Function in Newly Diagnosed Type 2 Diabetes With Severe Hyperglycemia After Short-Term Intensive Insulin Therapy. *Diabetes Care* **31**, 1927–1932 (2008).
6. Block, M. B., Rosenfield, R. L., Mako, M. E., Steiner, D. F. & Rubenstein, A. H. Sequential Changes in Beta-Cell Function in Insulin-Treated Diabetic Patients Assessed by C-Peptide Immunoreactivity. *N. Engl. J. Med.* **288**, 1144–1148 (1973).
7. Weng, J. *et al.* Effect of intensive insulin therapy on β-cell function and glycaemic control in patients with newly diagnosed type 2 diabetes: a multicentre randomised parallel-group trial. *The Lancet* **371**, 1753–1760 (2008).
8. Alvarsson, M. *et al.* Beneficial Effects of Insulin Versus Sulphonylurea on Insulin Secretion and Metabolic Control in Recently Diagnosed Type 2 Diabetic Patients. *Diabetes Care* **26**, 2231–2237 (2003).
9. Blum, B. *et al.* Functional beta-cell maturation is marked by an increased glucose threshold and by expression of urocortin 3. *Nat. Biotechnol.* **30**, 261–264 (2012).
10. Blum, B. *et al.* Reversal of β cell de-differentiation by a small molecule inhibitor of the TGFβ pathway. *eLife* **3**, (2014).
11. Rui, J. *et al.* β Cells that Resist Immunological Attack Develop during Progression of Autoimmune Diabetes in NOD Mice. *Cell Metab.* **25**, 727–738 (2017).
12. Talchai, C., Xuan, S., Lin, H. V., Sussel, L. & Accili, D. Pancreatic β Cell Dedifferentiation as a Mechanism of Diabetic β Cell Failure. *Cell* **150**, 1223–1234 (2012).
13. Cinti, F. *et al.* Evidence of β-Cell Dedifferentiation in Human Type 2 Diabetes. *J. Clin. Endocrinol. Metab.* **101**, 1044–1054 (2016).
14. Rakieten, N., Rakieten, M. L. & Nadkarni, M. V. Studies on the diabetogenic action of streptozotocin (NSC-37917). *Cancer Chemother. Rep.* **29**, 91–98 (1963).
15. Like, A. A. & Rossini, A. A. Streptozotocin-induced pancreatic insulitis: new model of diabetes mellitus. *Science* **193**, 415–417 (1976).
16. Thorel, F. *et al.* Conversion of adult pancreatic α-cells to β-cells after extreme β-cell loss. *Nature* **464**, 1149–1154 (2010).
17. Chera, S. *et al.* Diabetes recovery by age-dependent conversion of pancreatic δ-cells into insulin producers. *Nature* **514**, 503–507 (2014).
18. Brereton, M. F. *et al.* Reversible changes in pancreatic islet structure and function produced by elevated blood glucose. *Nat. Commun.* **5**, 4639 (2014).
19. Wang, Z., York, N. W., Nichols, C. G. & Remedi, M. S. Pancreatic β Cell Dedifferentiation in Diabetes and Redifferentiation following Insulin Therapy. *Cell Metab.* **19**, 872–882 (2014).
20. Tiano, J. P. & Mauvais-Jarvis, F. Importance of oestrogen receptors to preserve functional β-cell mass in diabetes. *Nat. Rev. Endocrinol.* **8**, 342–351 (2012).
21. Chon, S. & Gautier, J.-F. An Update on the Effect of Incretin-Based Therapies on β-Cell Function and Mass. *Diabetes Metab. J.* **40**, 99 (2016).

22. O'Neil, P. M. *et al.* Efficacy and safety of semaglutide compared with liraglutide and placebo for weight loss in patients with obesity: a randomised, double-blind, placebo and active controlled, dose-ranging, phase 2 trial. *The Lancet* **392**, 637–649 (2018).
23. Marso, S. P. *et al.* Semaglutide and Cardiovascular Outcomes in Patients with Type 2 Diabetes. *N. Engl. J. Med.* **375**, 1834–1844 (2016).
24. Drucker, D. J. Mechanisms of Action and Therapeutic Application of Glucagon-like Peptide-1. *Cell Metab.* **27**, 740–756 (2018).
25. Finan, B. *et al.* Targeted estrogen delivery reverses the metabolic syndrome. *Nat. Med.* **18**, 1847–1856 (2012).
26. Clemmensen, C. *et al.* Emerging hormonal-based combination pharmacotherapies for the treatment of metabolic diseases. *Nat. Rev. Endocrinol.* **15**, 90–104 (2019).
27. Waaseth, M. *et al.* Hormone replacement therapy use and plasma levels of sex hormones in the Norwegian Women and Cancer Postgenome Cohort – a cross-sectional analysis. *BMC Womens Health* **8**, (2008).
28. Bastidas-Ponce, A. *et al.* Foxa2 and Pdx1 cooperatively regulate postnatal maturation of pancreatic β-cells. *Mol. Metab.* (2017) doi:10.1016/j.molmet.2017.03.007.
29. Tritschler, S. *et al.* Concepts and limitations for learning developmental trajectories from single cell genomics. *Development* **146**, dev170506 (2019).
30. Haghverdi, L., Büttner, M., Wolf, F. A., Buettner, F. & Theis, F. J. Diffusion pseudotime robustly reconstructs lineage branching. *Nat. Methods* **13**, 845–848 (2016).
31. Nishimura, W. *et al.* A switch from MafB to MafA expression accompanies differentiation to pancreatic beta-cells. *Dev. Biol.* **293**, 526–539 (2006).
32. Bader, E. *et al.* Identification of proliferative and mature β-cells in the islets of Langerhans. *Nature* **535**, 430–434 (2016).
33. Roscioni, S. S., Migliorini, A., Gegg, M. & Lickert, H. Impact of islet architecture on β-cell heterogeneity, plasticity and function. *Nat. Rev. Endocrinol.* **12**, 695–709 (2016).
34. Ediger, B. N. *et al.* Islet-1 Is Essential for Pancreatic -Cell Function. *Diabetes* **63**, 4206–4217 (2014).
35. Gao, T. *et al.* Pdx1 Maintains β Cell Identity and Function by Repressing an α Cell Program. *Cell Metab.* **19**, 259–271 (2014).
36. Gu, C. *et al.* Pancreatic β Cells Require NeuroD to Achieve and Maintain Functional Maturity. *Cell Metab.* **11**, 298–310 (2010).
37. Gutiérrez, G. D. *et al.* Pancreatic β cell identity requires continual repression of non–β cell programs. *J. Clin. Invest.* **127**, 244–259 (2016).
38. Swisa, A. *et al.* PAX6 maintains β cell identity by repressing genes of alternative islet cell types. *J. Clin. Invest.* **127**, 230–243 (2016).
39. Taylor, B. L., Liu, F.-F. & Sander, M. Nkx6.1 Is Essential for Maintaining the Functional State of Pancreatic Beta Cells. *Cell Rep.* **4**, 1262–1275 (2013).
40. Kim-Muller, J. Y. *et al.* Aldehyde dehydrogenase 1a3 defines a subset of failing pancreatic β cells in diabetic mice. *Nat. Commun.* **7**, 12631 (2016).
41. Dahan, T. *et al.* Pancreatic β-Cells Express the Fetal Islet Hormone Gastrin in Rodent and Human Diabetes. *Diabetes* **66**, 426–436 (2017).
42. Solimena, M. *et al.* Systems biology of the IMIDIA biobank from organ donors and pancreatectomised patients defines a novel transcriptomic signature of islets from individuals with type 2 diabetes. *Diabetologia* **61**, 641–657 (2018).
43. Camunas-Soler, J. *et al.* Pancreas patch-seq links physiologic dysfunction in diabetes to single-cell transcriptomic phenotypes. *bioRxiv* (2019) doi:10.1101/555110.
44. Weir, G. C. & Bonner-Weir, S. Islet β cell mass in diabetes and how it relates to function, birth, and death: Islet β cell mass in diabetes. *Ann. N. Y. Acad. Sci.* **1281**, 92–105 (2013).

45. Qiu, W.-L. *et al.* Deciphering Pancreatic Islet β Cell and α Cell Maturation Pathways and Characteristic Features at the Single-Cell Level. *Cell Metab.* **25**, 1194-1205.e4 (2017).
46. Wolf, F. A. *et al.* PAGA: graph abstraction reconciles clustering with trajectory inference through a topology preserving map of single cells. *Genome Biol.* **20**, (2019).
47. Taniguchi, C. M., Emanuelli, B. & Kahn, C. R. Critical nodes in signalling pathways: insights into insulin action. *Nat. Rev. Mol. Cell Biol.* **7**, 85–96 (2006).
48. Rowlands, J., Heng, J., Newsholme, P. & Carlessi, R. Pleiotropic Effects of GLP-1 and Analogs on Cell Signaling, Metabolism, and Function. *Front. Endocrinol.* **9**, 672 (2018).
49. Cheatham, B. & Kahn, C. R. Insulin action and the insulin signaling network. *Endocr. Rev.* **16**, 117–142 (1995).
50. Segars, J. H. & Driggers, P. H. Estrogen action and cytoplasmic signaling cascades. Part I: membrane-associated signaling complexes. *Trends Endocrinol. Metab. TEM* **13**, 349–354 (2002).
51. Hancock, M. L. *et al.* Insulin Receptor Associates with Promoters Genome-wide and Regulates Gene Expression. *Cell* **177**, 722-736.e22 (2019).
52. Kulkarni, R. N. *et al.* Altered function of insulin receptor substrate-1–deficient mouse islets and cultured β-cell lines. *J. Clin. Invest.* **104**, R69–R75 (1999).
53. Ueki, K. *et al.* Total insulin and IGF-I resistance in pancreatic β cells causes overt diabetes. *Nat. Genet.* **38**, 583–588 (2006).
54. Fonseca, S. G., Gromada, J. & Urano, F. Endoplasmic reticulum stress and pancreatic β-cell death. *Trends Endocrinol. Metab.* (2011) doi:10.1016/j.tem.2011.02.008.
55. Diaferia, G. R., Cirulli, V. & Biunno, I. SEL1L Regulates Adhesion, Proliferation and Secretion of Insulin by Affecting Integrin Signaling. *PLoS ONE* **8**, e79458 (2013).
56. Francisco, A. B. *et al.* Haploid Insufficiency of Suppressor Enhancer Lin12 1-like (SEL1L) Protein Predisposes Mice to High Fat Diet-induced Hyperglycemia. *J. Biol. Chem.* **286**, 22275–22282 (2011).
57. Hassler, J. R. *et al.* The IRE1α/XBP1s Pathway Is Essential for the Glucose Response and Protection of β Cells. *PLOS Biol.* **13**, e1002277 (2015).
58. Hu, Y. *et al.* Endoplasmic Reticulum–Associated Degradation (ERAD) Has a Critical Role in Supporting Glucose-Stimulated Insulin Secretion in Pancreatic β-Cells. *Diabetes* **68**, 733–746 (2019).
59. Sims, E. K. *et al.* Elevations in the Fasting Serum Proinsulin-to-C-Peptide Ratio Precede the Onset of Type 1 Diabetes. *Diabetes Care* **39**, 1519–1526 (2016).
60. Tersey, S. A. *et al.* Islet β-cell endoplasmic reticulum stress precedes the onset of type 1 diabetes in the nonobese diabetic mouse model. *Diabetes* **61**, 818–827 (2012).
61. Xu, B. *et al.* Estrogens Promote Misfolded Proinsulin Degradation to Protect Insulin Production and Delay Diabetes. *Cell Rep.* **24**, 181–196 (2018).
62. Tiwari, A. *et al.* SDF2L1 interacts with the ER-associated degradation machinery and retards the degradation of mutant proinsulin in pancreatic β-cells. *J. Cell Sci.* **126**, 1962–1968 (2013).
63. Sasako, T. *et al.* Hepatic Sdf2l1 controls feeding-induced ER stress and regulates metabolism. *Nat. Commun.* **10**, 947 (2019).
64. Ho, D. V. & Chan, J. Y. Induction of Herpud1 expression by ER stress is regulated by Nrf1. *FEBS Lett.* **589**, 615–620 (2015).
65. Wong, N., Morahan, G., Stathopoulos, M., Proietto, J. & Andrikopoulos, S. A novel mechanism regulating insulin secretion involving Herpud1 in mice. *Diabetologia* **56**, 1569–1576 (2013).
66. Laybutt, D. R. *et al.* Endoplasmic reticulum stress contributes to beta cell apoptosis in type 2 diabetes. *Diabetologia* **50**, 752–763 (2007).
67. Oda, Y. *et al.* Derlin-2 and Derlin-3 are regulated by the mammalian unfolded protein response and are required for ER-associated degradation. *J. Cell Biol.* **172**, 383–393 (2006).
68. Belmont, P. J. *et al.* Roles for endoplasmic reticulum-associated degradation and the novel

endoplasmic reticulum stress response gene Derlin-3 in the ischemic heart. *Circ. Res.* **106**, 307–316 (2010).
69. Zhu, D. *et al.* Single-Cell Transcriptome Analysis Reveals Estrogen Signaling Coordinately Augments One-Carbon, Polyamine, and Purine Synthesis in Breast Cancer. *Cell Rep.* **25**, 2285-2298.e4 (2018).
70. Torrent, M., Chalancon, G., de Groot, N. S., Wuster, A. & Madan Babu, M. Cells alter their tRNA abundance to selectively regulate protein synthesis during stress conditions. *Sci. Signal.* **11**, eaat6409 (2018).
71. Xu, G. *et al.* Downregulation of GLP-1 and GIP Receptor Expression by Hyperglycemia: Possible Contribution to Impaired Incretin Effects in Diabetes. *Diabetes* **56**, 1551–1558 (2007).
72. Fritsche, A., Stefan, N., Hardt, E., Häring, H. & Stumvoll, M. Characterisation of beta-cell dysfunction of impaired glucose tolerance: Evidence for impairment of incretin-induced insulin secretion. *Diabetologia* **43**, 852–858 (2000).
73. Kjems, L. L., Holst, J. J., Vølund, A. & Madsbad, S. The influence of GLP-1 on glucose-stimulated insulin secretion: effects on beta-cell sensitivity in type 2 and nondiabetic subjects. *Diabetes* **52**, 380–386 (2003).
74. Guo, S. *et al.* Inactivation of specific β cell transcription factors in type 2 diabetes. *J. Clin. Invest.* **123**, 3305–3316 (2013).
75. Jonas, J. C. *et al.* Chronic hyperglycemia triggers loss of pancreatic beta cell differentiation in an animal model of diabetes. *J. Biol. Chem.* **274**, 14112–14121 (1999).
76. Laybutt, D. R. *et al.* Genetic Regulation of Metabolic Pathways in β-Cells Disrupted by Hyperglycemia. *J. Biol. Chem.* **277**, 10912–10921 (2002).
77. Keenan, H. A. *et al.* Residual Insulin Production and Pancreatic -Cell Turnover After 50 Years of Diabetes: Joslin Medalist Study. *Diabetes* **59**, 2846–2853 (2010).
78. Lam, C. J., Chatterjee, A., Shen, E., Cox, A. R. & Kushner, J. A. Low Level Insulin Content Within Abundant Non-Beta Islet Endocrine Cells in Long-Standing Type 1 Diabetes. *Diabetes* db180305 (2018) doi:10.2337/db18-0305.
79. Seiron, P. *et al.* Characterisation of the endocrine pancreas in type 1 diabetes: islet size is maintained but islet number is markedly reduced. *J. Pathol. Clin. Res.* **5**, 248–255 (2019).
80. Zhou, Q. & Melton, D. A. Pancreas regeneration. *Nature* **557**, 351–358 (2018).
81. Wolf, F. A., Angerer, P. & Theis, F. J. SCANPY: large-scale single-cell gene expression data analysis. *Genome Biol.* **19**, (2018).
82. Büttner, M., Miao, Z., Wolf, F. A., Teichmann, S. A. & Theis, F. J. A test metric for assessing single-cell RNA-seq batch correction. *Nat. Methods* **16**, 43–49 (2019).
83. Blondel, V. D., Guillaume, J.-L., Lambiotte, R. & Lefebvre, E. Fast unfolding of communities in large networks. *J. Stat. Mech. Theory Exp.* **2008**, P10008 (2008).
84. Becht, E. *et al.* Dimensionality reduction for visualizing single-cell data using UMAP. *Nat. Biotechnol.* **37**, 38–44 (2018).
85. Chiang, M.-K. & Melton, D. A. Single-Cell Transcript Analysis of Pancreas Development. *Dev. Cell* **4**, 383–393 (2003).
86. Katsuta, H. *et al.* Single pancreatic beta cells co-express multiple islet hormone genes in mice. *Diabetologia* **53**, 128–138 (2010).
87. Alpert, S., Hanahan, D. & Teitelman, G. Hybrid insulin genes reveal a developmental lineage for pancreatic endocrine cells and imply a relationship with neurons. *Cell* **53**, 295–308 (1988).
88. Zheng, G. X. Y. *et al.* Massively parallel digital transcriptional profiling of single cells. *Nat. Commun.* **8**, 14049 (2017).
89. Wolock, S. L., Lopez, R. & Klein, A. M. Scrublet: Computational Identification of Cell Doublets in Single-Cell Transcriptomic Data. *Cell Syst.* **8**, 281-291.e9 (2019).
90. Kowalczyk, M. S. *et al.* Single-cell RNA-seq reveals changes in cell cycle and differentiation

programs upon aging of hematopoietic stem cells. *Genome Res.* **25**, 1860–1872 (2015).
91. Tirosh, I. *et al.* Dissecting the multicellular ecosystem of metastatic melanoma by single-cell RNA-seq. *Science* **352**, 189–196 (2016).
92. Satija, R., Farrell, J. A., Gennert, D., Schier, A. F. & Regev, A. Spatial reconstruction of single-cell gene expression data. *Nat. Biotechnol.* **33**, 495–502 (2015).
93. Law, C. W., Chen, Y., Shi, W. & Smyth, G. K. voom: precision weights unlock linear model analysis tools for RNA-seq read counts. *Genome Biol.* **15**, R29 (2014).
94. Ritchie, M. E. *et al.* limma powers differential expression analyses for RNA-sequencing and microarray studies. *Nucleic Acids Res.* **43**, e47–e47 (2015).
95. Soneson, C. & Robinson, M. D. Bias, robustness and scalability in single-cell differential expression analysis. *Nat. Methods* **15**, 255–261 (2018).
96. Kuleshov, M. V. *et al.* Enrichr: a comprehensive gene set enrichment analysis web server 2016 update. *Nucleic Acids Res.* **44**, W90–W97 (2016).
97. Polański, K. *et al.* BBKNN: Fast Batch Alignment of Single Cell Transcriptomes. *Bioinforma. Oxf. Engl.* (2019) doi:10.1093/bioinformatics/btz625.
98. La Manno, G. *et al.* RNA velocity of single cells. *Nature* **560**, 494–498 (2018).

Fig. 1

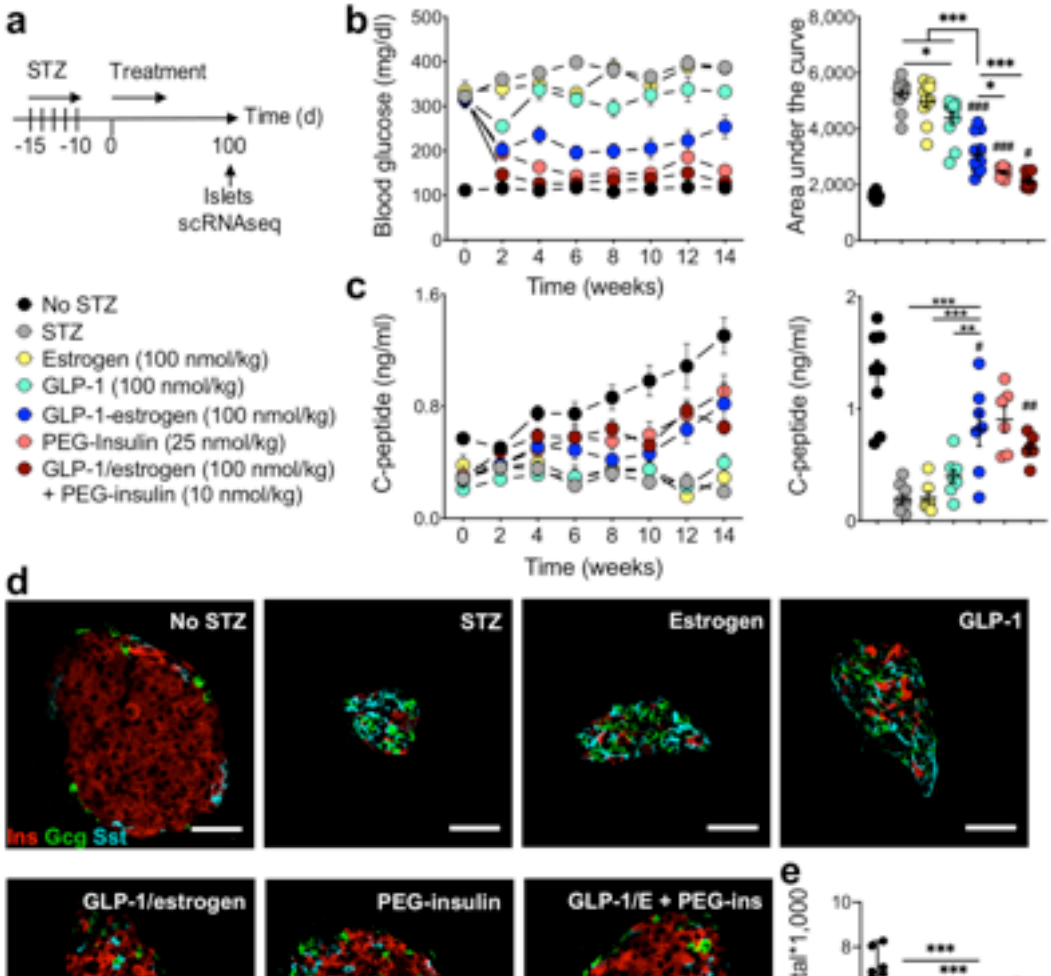

f

Treatment	Islets (n)	Insulin cells/ total cells	Glucagon cells/ total cells	Somatostatin cells/ total cells	Cells/islet
No STZ	196	0.77 ± 0.01	0.19 ± 0.01	0.05 ± 0.00	288.71 ± 17.68
STZ	180	0.26 ± 0.02 *** &&& §§§	0.61 ± 0.02 *** &&& §§§	0.15 ± 0.01 *** &&&	118.57 ± 6.28 **
Estrogen	177	0.37 ± 0.02 ***	0.51 ± 0.02 ***	0.15 ± 0.02 *** §§§	114.15 ± 6.30 *** §
GLP-1	199	0.41 ± 0.01 ***	0.48 ± 0.01 ***	0.11 ± 0.01	141.42 ± 7.76
GLP-1/estrogen	175	0.52 ± 0.01 ###	0.39 ± 0.01 ###	0.09 ± 0.01	156.66 ± 8.85 $ ###
PEG-insulin	119	0.53 ± 0.01 ###	0.40 ± 0.01 ###	0.07 ± 0.01	152.31 ± 8.41 $ ###
GLP-1/estrogen + PEG-insulin	166	0.53 ± 0.01 ###	0.40 ± 0.01 ###	0.08 ± 0.01 #	204.63 ± 13.00 ###

Figure 1: GLP-1/estrogen and PEG-insulin treatment regenerates functional β-cell mass. (a) 8-week old C57Bl6/J mice were treated with daily subcutaneous injections of either vehicle (n=12, no STZ), vehicle (n=13, STZ), a GLP-1 analog (n=11), estrogen (n=11), the GLP-1/estrogen conjugate (n=11), PEG-insulin (n=9), or GLP-1/estrogen and PEG-insulin (n=10) ten days after the last STZ injection at the indicated doses for 100 days. Effects on fasting **(b)** blood glucose and **(c)** C-peptide levels of treated mice. Data are mean ± SEM. *P < 0.05, **P < 0.01, ***P < 0.001, among STZ, estrogen, GLP-1 and GLP-1/estrogen treated mice (one-way ANOVA with Tukey post-hoc test; F (DFn, DFd) = F (3, 42) = 24.09). *P < 0.05, **P < 0.01, ***P < 0.001 to compound injections; #P < 0.01, ###P < 0.001 to no STZ mice, comparing no STZ, GLP-1/estrogen, PEG-insulin, and co-treated mice (one-way ANOVA and Tukey post-hoc; DF=31, F (3, 38) = 29.32). **(d)** Immunostaining for insulin, glucagon, and somatostatin of pancreatic sections shows effects on islet architecture after 100 days of treatment. **(e)** Quantitative comparison of total insulin area in pancreatic sections (No STZ; 25 sections of n=3 mice), vehicle (STZ; 21, n=3 mice), estrogen (27, n=3 mice), GLP-1 (26, n=3 mice), GLP-1/estrogen (18, n=2 mice), PEG-insulin (24, n=3 mice), or GLP-1/estrogen and PEG-insulin co-therapy (27, n=3 mice). **P < 0.01, ***P < 0.001, among STZ, estrogen, GLP-1 and GLP-1/estrogen treated mice (one-way ANOVA with Tukey post-hoc test; F (3, 88) = 17.66). #P < 0.05, among GLP-1/estrogen, PEG-insulin, and co-treated mice (one-way ANOVA with Tukey post-hoc; F (2, 66) = 4.56). **(f)** Cell composition of endocrine islets in the end of the study (No STZ: 196 islets of n=3 mice; STZ: 180, n=3; Estrogen: 177, n=3; GLP-1: 199, n=3; GLP-1/estrogen: 175, n=2; PEG-insulin: 119, n=3; co-therapy: 166, n=3). Data are mean ± SEM. **P < 0.01 and ***P < 0.001 indicate significance to GLP-1/estrogen treated mice. &&&P < 0.001 indicates significance to estrogen treated mice. §P < 0.05 and §§§P < 0.001 indicate significance to GLP-1 treated mice. $P < 0.05 indicates significance to GLP-1/estrogen plus PEG-insulin treatment. #P < 0.05 and ###P < 0.001 indicates significance to healthy controls. One-way ANOVA with Tukey post-hoc ($F_{β\text{-cells}}$ (6, 1187) = 175.7; $F_{α\text{-cells}}$ (6, 1202) = 124.7; $F_{δ\text{-cells}}$ (6, 1145) = 44.76).

Fig. 2

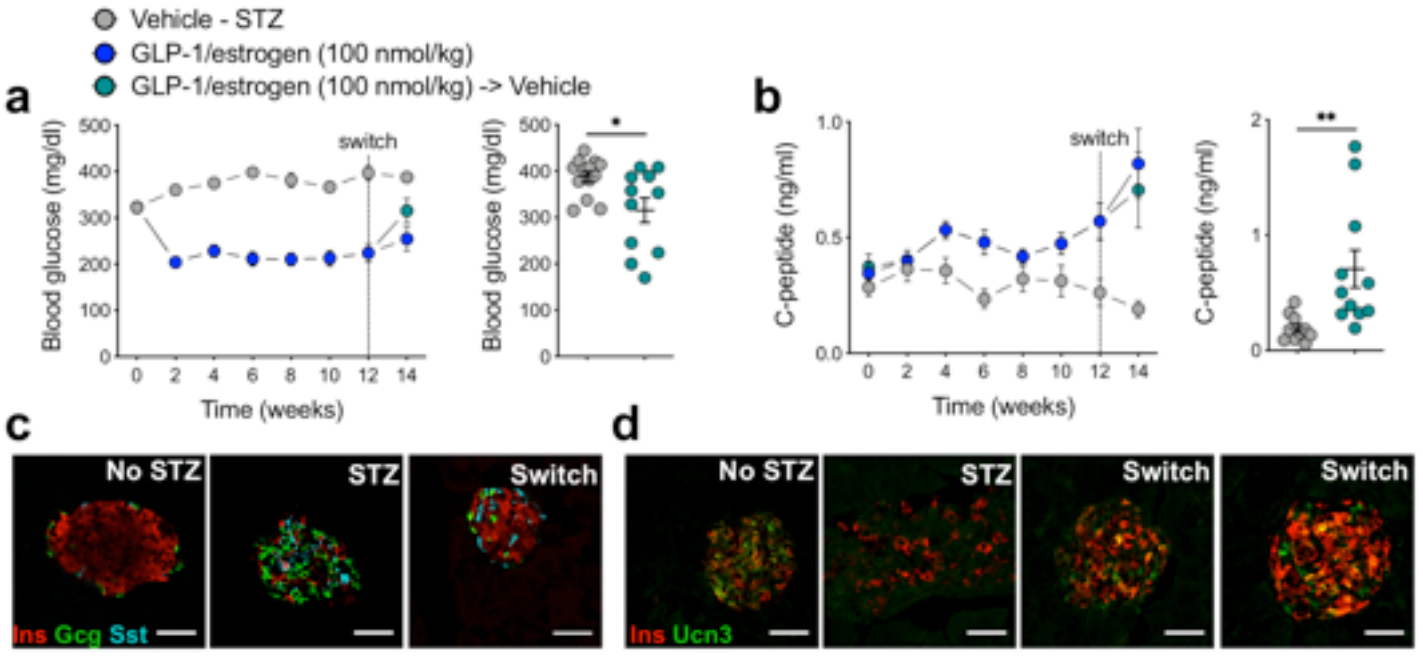

Figure 2: Sustained effects of GLP-1/estrogen to ameliorate mSTZ diabetes in mice. A group of GLP-1/estrogen treated mice were switched from daily GLP-1/estrogen treatment for 12 weeks to vehicle treatment for another two weeks. **(a)** Fasting blood glucose at week 14 (*P < 0.05, unpaired two-sided t-test; t=2.623, df=22). **(b)** Fasting C-peptide levels at week 14 (*P < 0.05, unpaired two-sided t-test; t=2.939, df=19). **(c)** Immunohistochemistry of representative pancreatic islets. **(d)** Ucn3 immunohistochemistry at week 14.

Fig. 3

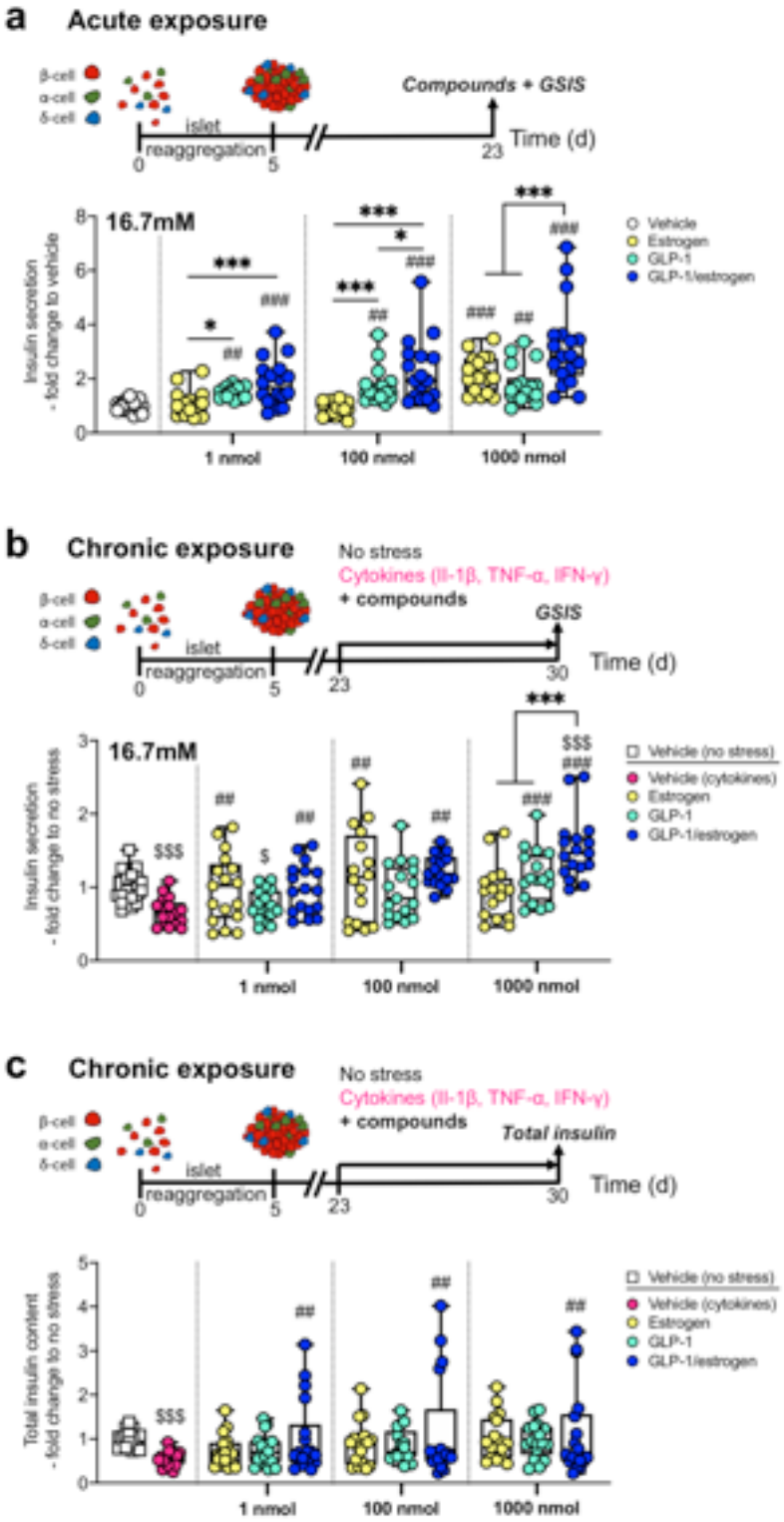

Figure 3: GLP-1/estrogen improves function of human micro-islets. a) Insulin secretion of human micro-islets after acute exposure to either vehicle, estrogen, GLP-1, or the GLP-1/estrogen conjugate at three escalating doses at a glucose concentration of 16.7mM. N= 5-6 micro-islets of n=3 human donors for each condition. Secretion (mean±SEM) of donor1 = 0.36±0.01 ng/ml, donor1 = 0.37±0.02 ng/ml, and donor3 = 0.29±0.03 ng/ml after vehicle exposure. $^{\#\#}$P<0.01, $^{\#\#\#}$P<0.001, to vehicle treatment. *P<0.05, **P<0.01, ***P<0.001, among compound treatments. Significance by one-way ANOVA with donor as random effect followed by Tukey post-hoc ($F_{low\ dose}(3, 65) = 14.04$; $F_{medium\ dose}(3, 64) = 18.59$; $F_{high\ dose}(3, 66) = 25.50$). Boxplot of all data points. **b)** Insulin secretion of human micro islets after 7-day exposure to cytokine stress and effect of either estrogen, GLP-1, or GLP-1/estrogen treatment. Secretion (mean±SEM) of donor1 = 0.13±0.02 ng/ml, donor2 = 0.56±0.04 ng/ml, and donor3 = 0.51±0.06 ng/ml after chronic vehicle (no stress) exposure. $^{\$\$\$}$P<0.001, between healthy and cytokine exposed islets (unpaired two-sided t-test; t=4.779, df=33). $^{\#\#}$P<0.01, $^{\#\#\#}$P<0.001, to cytokine exposed islets. *P<0.05, ***P<0.001, among treatments. $^{\$}$P<0.05, $^{\$\$\$}$P<0.001, to healthy islets. Significance by one-way ANOVA with donor as random effect followed by Tukey post-hoc ($F_{low\ dose}(4, 79) = 6.49$; $F_{medium\ dose}(4, 78) = 7.58$; $F_{high\ dose}(4, 78) = 22.51$). N= 5-6 micro-islets of n=3 human donors for each condition. Boxplot of all data points. c) Total insulin content of human micro islets after 7-day exposure to cytokine stress and effect of either estrogen, GLP-1, or GLP-1/estrogen treatment. Insulin content (mean±SEM) of donor1 = 41.11±3.73 ng/islet, donor2 = 30.86±3.36 ng/islet, and donor3 = 82.73±3.99 ng/islet after chronic vehicle (no stress) exposure. $^{\$\$\$}$P<0.001, between healthy and cytokine exposed islets (unpaired two-sided t-test; t=7.429, df=32). $^{\#\#}$P<0.01, to cytokine exposed islets. Significance by one-way ANOVA with donor as random effect followed by Tukey post-hoc ($F_{low\ dose}(4, 80) = 4.12$; $F_{medium\ dose}(4, 78) = 3.01$; $F_{high\ dose}(4, 79) = 3.31$). N= 5-6 micro-islets of n=3 human donors for each condition. Boxplot of all data points

Fig. 4

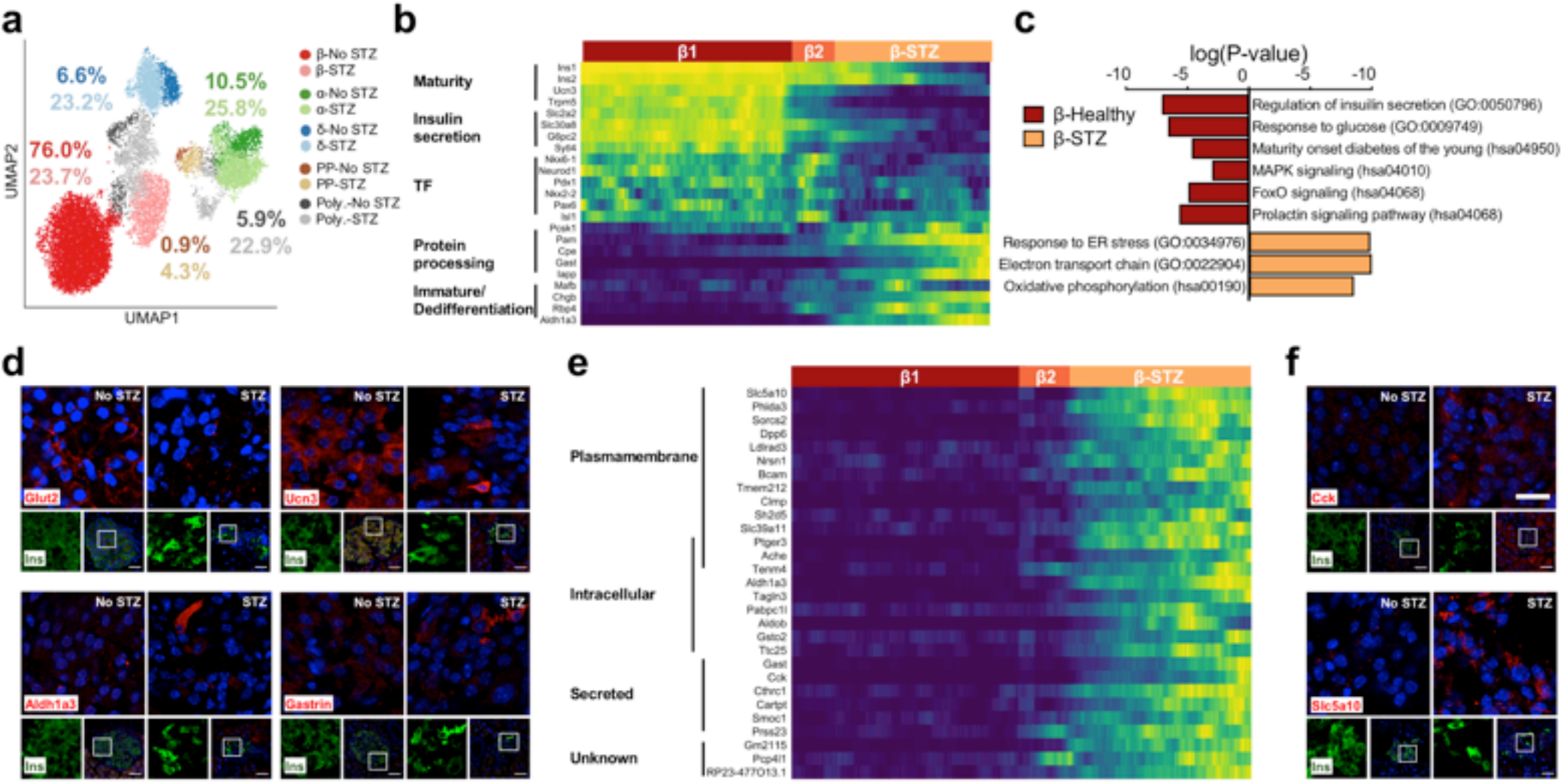

Figure 4: Novel β-cell dedifferentiation markers in STZ-diabetic mice. (a) UMAP plot of 12430 cells from healthy and STZ-treated mice. Colors highlight endocrine cell clusters, whereby color tone distinguishes no STZ (dark colors) or STZ treatment (light colors). Values indicate the proportions of each cell cluster in no STZ or STZ treatment, respectively. **(b)** Gene expression changes of representative markers of β-cell identity, maturation and function along the trajectory from mature (β1) to immature (β2) to β-cells from mSTZ treated mice (β-STZ) indicating a continuous transition. Cells are ordered based on a random-walk-based cell-to-cell distance metric. Expression is shown as the running average along the inferred trajectory scaled to the maximum observed level per gene. β1-cells were downsampled to 1500 cells for better visualization. **(c)** GO term and KEGG pathway enrichment analysis of significantly up- and downregulated genes in β-cells of STZ-treated mice compared to β-cells of healthy mice (absolute log fold change > 0.25, FDR < 0.01; selective pathways are depicted, see also Supplemental Table 3). **(d)** Immunohistochemical analysis of Glut2, Ucn3, Aldh1a3, and Gastrin in β-cells of STZ healthy mice at study end. All scale bars, 50 µm. **(e)** Gene expression along the trajectory from β1 to β-STZ as in (c) of 29 genes specifically expressed in β-cells from mSTZ treated mice (expression in <5% of no-STZ β-cells and >25% of mSTZ β-cells, M&M). Cellular locations of associated proteins are indicated. **(f)** Immunohistochemical analysis of Cck and Slc5a10 in β-cells of STZ and healthy mice at study end. All scale bars, 50 µm.

Fig. 5

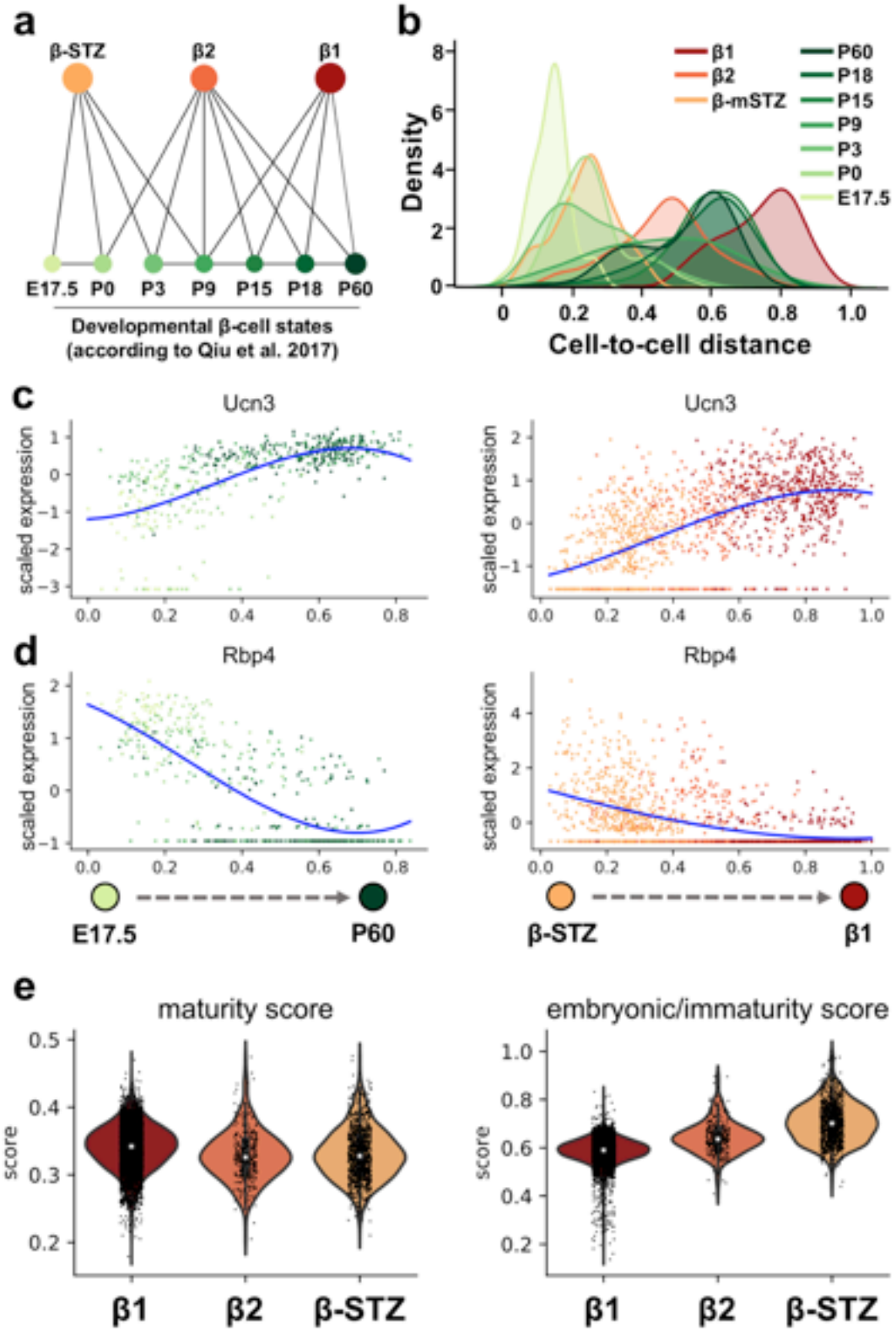

Figure 5: mSTZ derived β-cells are similar to immature β-cells from embryonic/neonatal islets. (a) Transcriptional similarity of β-cell subpopulations and β-cells sampled between E17.5 and P60 inferred based on a measure for cluster connectivity using PAGA. Edge weights indicate significance. Edge weight > 0.7 are shown. **(b)** Cell density of β-cell clusters along a cellular trajectory reflecting β-cell maturation. Cells are ordered based on a random-walk based cell-to-cell distance metric. Data sets were integrated by computing a common single-cell neighborhood graph (Polański et al. 2019). **(c-d)** Expression of a β-cell maturity (c) and immaturity (d) marker along the inferred trajectory in (b). Left panel shows β-cell subpopulations sampled between E17.5 and P60, right panel shows β-cell subpopulations from healthy and mSTZ-treated mice. Dots show expression levels of individual cells colored by β-cell subpopulations. Red lines approximate expression along the trajectory by polynominal regression fits. **(e)** Violin plots showing the distribution of cell scores characteristic for β-cell maturity (left) and embryonic-like/immaturity(right). Scores were calculated based on differentially expressed genes between clusters of mature (P60) and embryonic/immature (E17.5/P0) cells.

Fig. 6

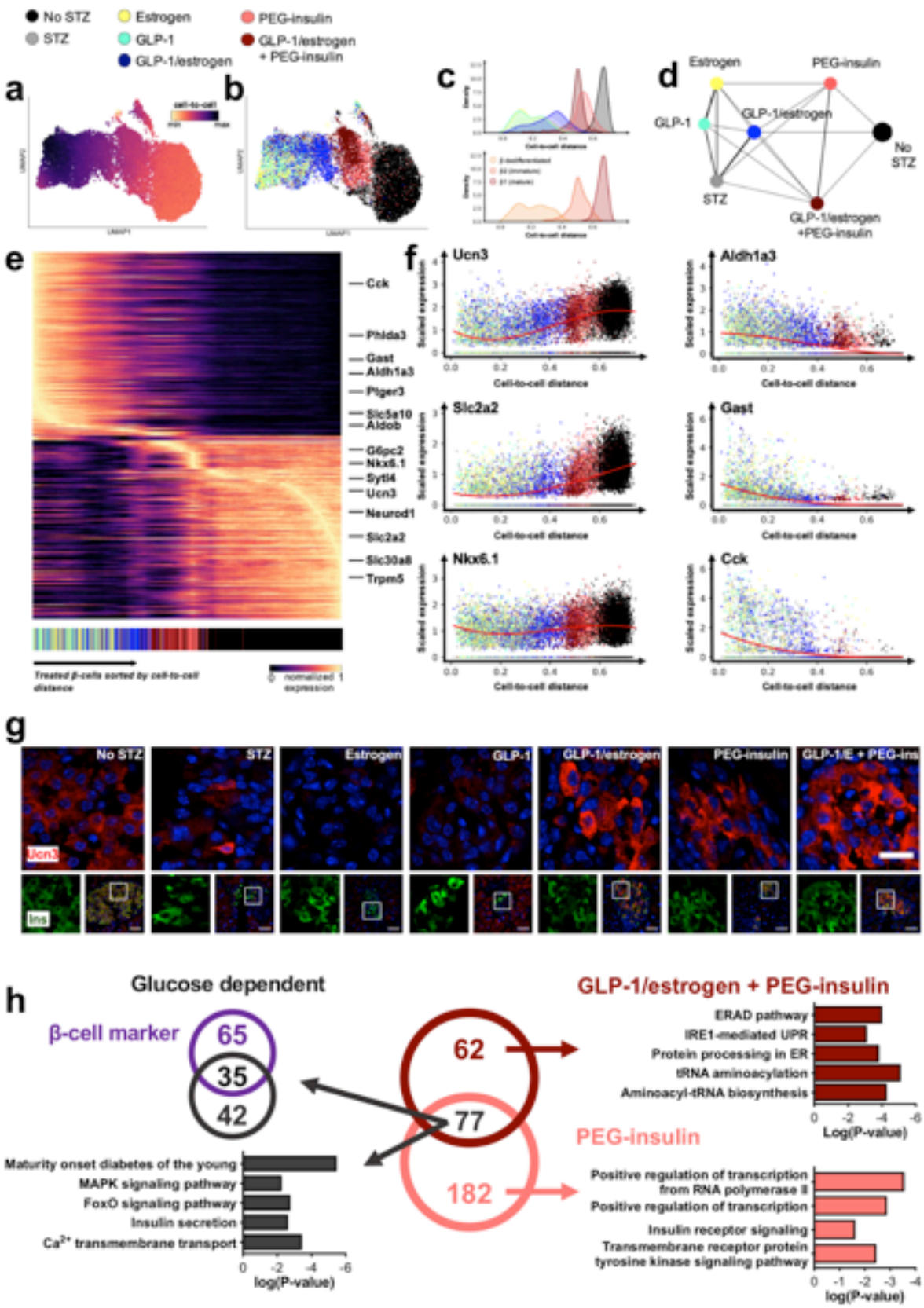

Figure 6: β-cell redifferentiation upon insulin and GLP-1/estrogen treatment. (a-b) UMAP plot of β-cells from all treatment groups. Color indicates **(a)** random-walk-based cell-to-cell distance and **(b)** treatment groups. Cell density of treatment groups **(c)** and β-cell subpopulations along a cell trajectory from dedifferentiated to mature β-cells indicating the redifferentiation state. Cells are ordered according to a random-walk-based cell-to-cell distance as shown in (a). **(d)** Abstracted graph of transcriptomic similarity of β-cells between treatment groups inferred based on a measure for cluster connectivity using PAGA. Edge weight indicates link significance. **(e)** Gene expression changes of top 200 up- and downregulated genes in β-cells of STZ-treated mice along the cell trajectory from a dedifferentiated to mature state as in (c, d). Expression is shown as the running average scaled to the maximum observed level per gene. Genes are ordered by their maximum expression. The bar at the bottom shows the location of individual cells colored by treatment group. **(f)** Expression of selected β-cell maturity and dedifferentiation markers along the cell-to-cell distance. Dots show expression levels of individual cells colored by treatment group, superimposed red lines are polynomial regression fits. **(g)** Immunohistochemical analysis of β-cell maturity marker Ucn3. Scale bar, 50 µm. **(h)** Venn diagram showing the number of upregulated genes (log fold change > 0.25, FDR < 0.01) specifically in β-cells of PEG-insulin and GLP-1/estrogen plus PEG-insulin co-treated mice compared STZ treated mice (left). Selected GO terms and KEGG pathways are depicted.

Fig. 7

a

	β-cells	α-cells	δ-cells	PP-cells	Poly.-cells
No STZ	18/5643 (0.32 %)	0/781 (0 %)	0/493 (0 %)	0/70 (0 %)	2/436 (0.46 %)
STZ	4/1186 (0.34 %)	2/617 (0.32 %)	0/218 (0 %)	0/118 (0 %)	4/2870 (0.14 %)
Estrogen	8/1147 (0.7 %)	3/384 (0.78 %)	1/606 (0.17 %)	0/45 (0 %)	2/2459 (0.08 %)
GLP-1	3/795 (0.38 %)	2/683 (0.29 %)	1/972 (0.1 %)	0/308 (0 %)	11/1140 (0.96 %)
GLP-1/estrogen	3/1345 (0.22 %)	2/1328 (0.15 %)	0/1249 (0 %)	0/242 (0 %)	7/1061 (0.66 %)
PEG-insulin	3/998 (0.3 %)	0/660 (0 %)	0/558 (0 %)	0/190 (0 %)	2/852 (0.23 %)
GLP-1/E + PEG-ins	14/1239 (1.13 %)	0/588 (0 %)	3/616 (0.49 %)	0/136 (0 %)	7/696 (1.01 %)

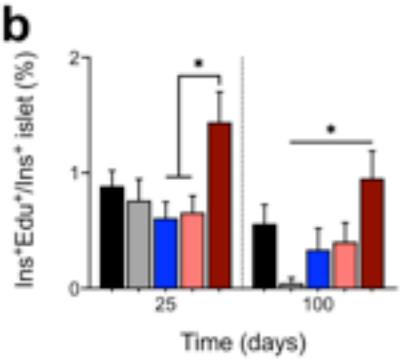

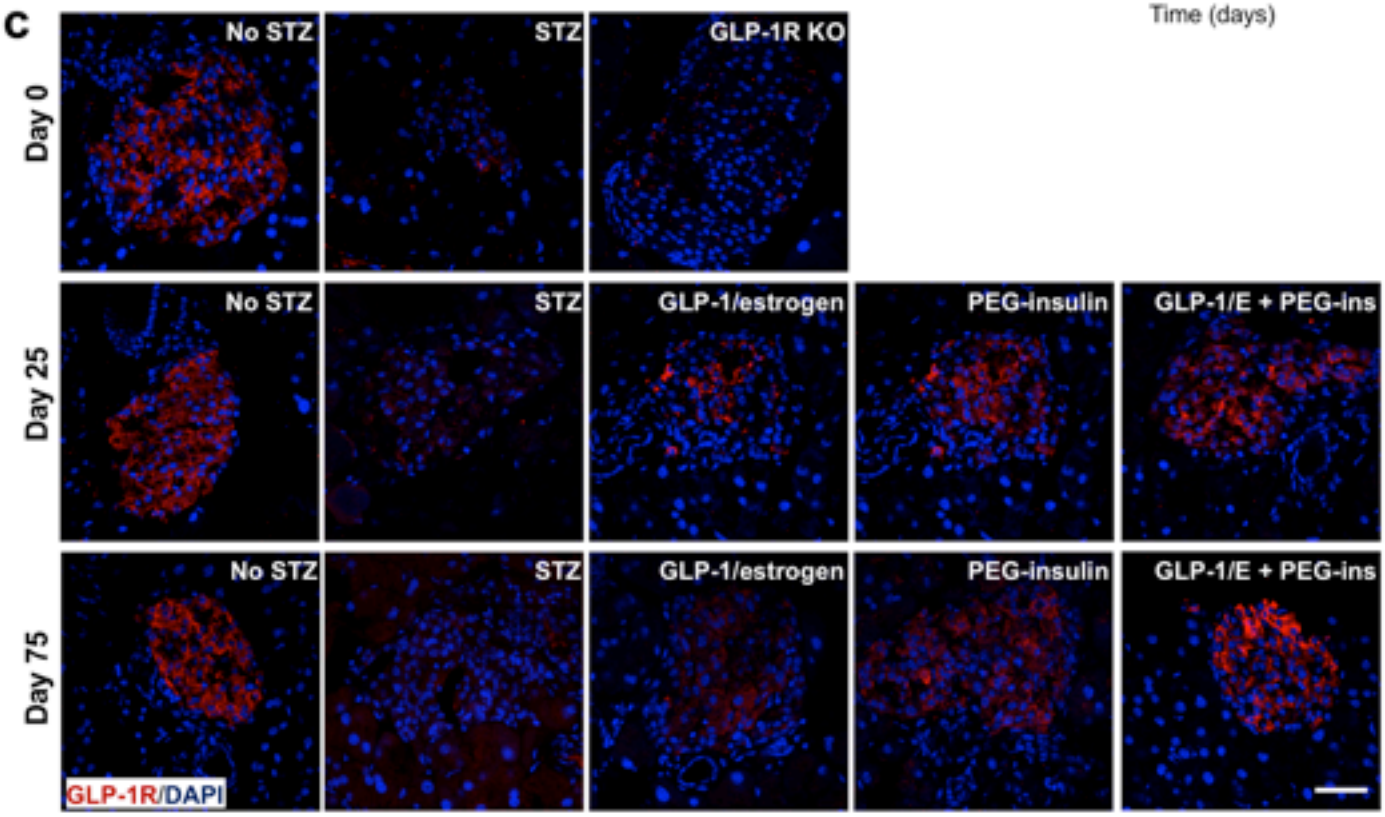

Figure 7: Treatment specific effects of β-cell regeneration. (a-b) Contribution of β-cell proliferation to β-cell regeneration after drug treatment of mSTZ mice. **(a)** ScRNA-seq of endocrine cells after 100 days of treatment suggests an increased proliferation of specifically beta cells after GLP-1/estrogen and PEG-insulin co-treatment. **(b)** Increased rate of proliferating β-cells as indicated by EdU^+ β-cell per islet in no STZ, STZ, GLP-1/estrogen, PEG-insulin, and co-treated mice after 25 and 100 days of treatment. Day 25: No STZ, 73 islets of n=3 mice; STZ, 36 islets, n=3; GLP-1/estrogen, 37 islets, n=3; PEG-insulin, 61 islets, n=3; GLP-1/estrogen and PEG-insulin, 50 islets, n=3. Day 100: No STZ, 47 islets of n=3 mice; STZ, 47 islets, n=3; GLP-1/estrogen, 36 islets, n=2; PEG-insulin, 43 islets, n=3; GLP-1/estrogen and PEG-insulin, 47 islets, n=3. Data are mean ± SEM. *P<0.05, comparing indicated treatments at either day 25 or day 100 by one-way ANOVA followed by Tukey post-hoc comparison (F_{D25} (4, 247) = 3.413; F_{D100} (4, 211) = 4.037). **(c)** Immunohistochemical analysis of GLP-1R expression. A GLP-1R knock-out (GLP-1R KO) mouse was used to show specificity of GLP-1R antibody within the islet of Langerhans. Scale bar, 50 μm.

Fig. 8

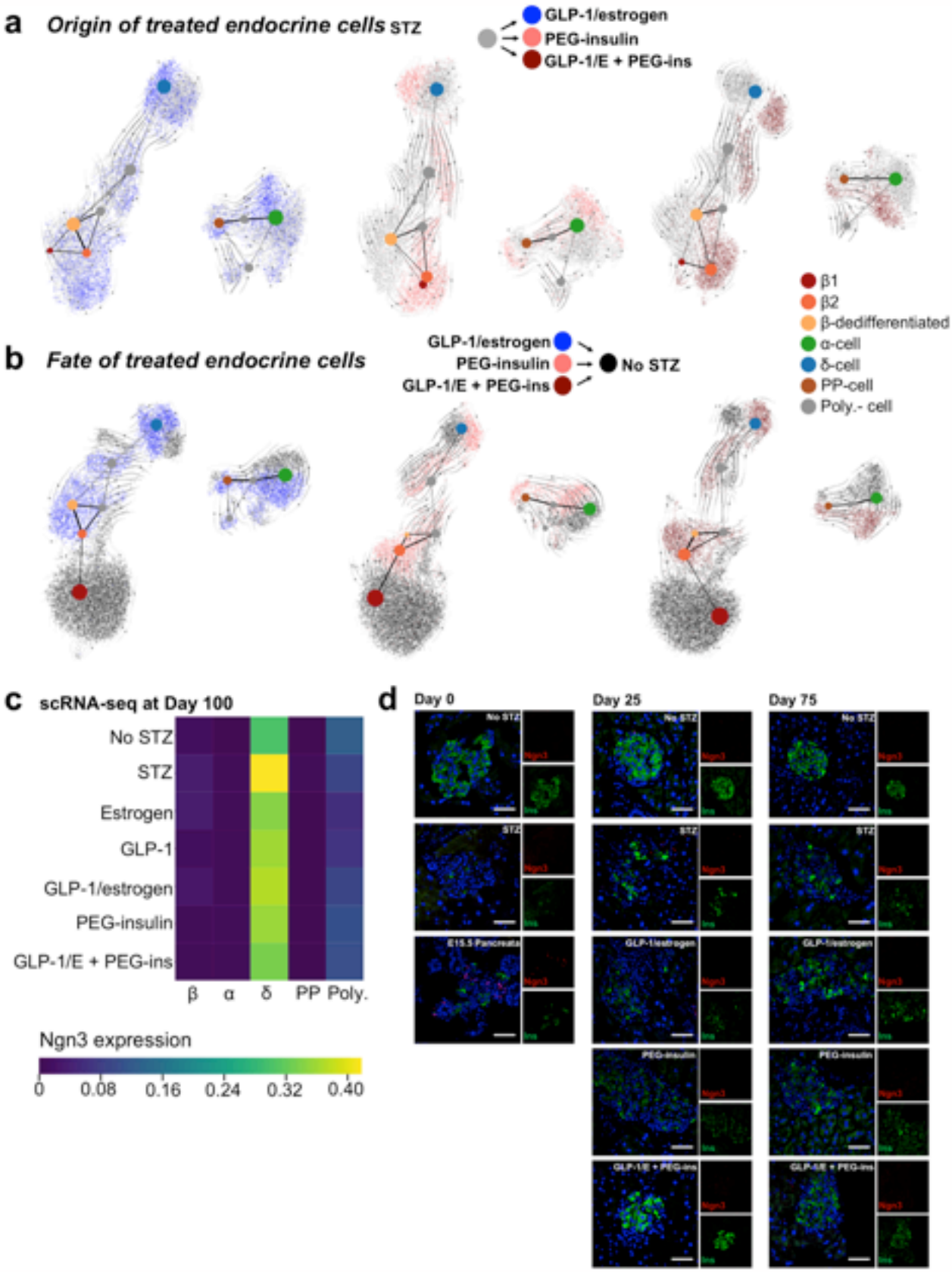

Figure 8: Origin and fate of treated endocrine cells. (a-b) Cluster relationships and cell transitions indicating the origin and fate of treated endocrine cells. Graphs of lineage relationships are derived from cluster connectivity using PAGA. Paths in the graph signify potential lineage transitions and are weighted by significance. Cell transitions are inferred from estimated RNA velocities and the direction of movement plotted as streamlines on the UMAP. **(a)** Plots including endocrine cells from mSTZ and GLP-1/estrogen (left), PEG-insulin (middle) or GLP-1/estrogen plus PEG-insulin (right) treated mice, respectively, showing movement from mSTZ (origin/starting point) towards treated cells. **(b)** Plots including endocrine cells from healthy and GLP-1/estrogen (left), PEG-insulin (middle) or GLP-1/estrogen plus PEG-insulin (right) treated mice, respectively, showing a potential movement of the treated cells towards healthy cells (fate). **(c-d)** Expression of the endocrine progenitor marker Ngn3 to assess contribution of β-cell neogenesis to β-cell regeneration by GLP-1/estrogen, PEG-insulin, and GLP-1/estrogen plus PEG-insulin treatment. **(c)** ScRNA-seq showed no increase of Ngn3 expression in endocrine cells after 100 days of treatment. **(d)** Immunohistochemistry of Ngn3 expression during the course of the study. Mouse E15.5 pancreas was used as positive control and shows nuclear staining for Ngn3.

Extended Data Fig. 1

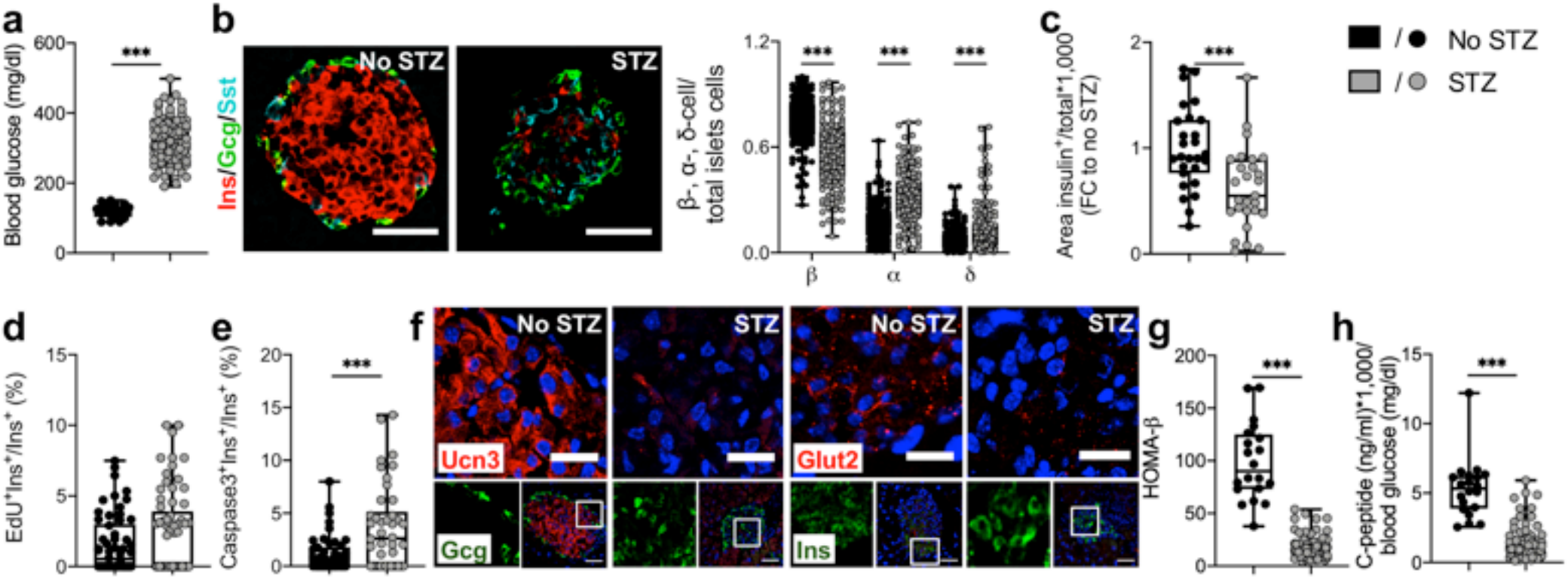

Extended Data Figure 1: Remaining β-cells lose cell identity 10 days after last STZ injection. Effects of either vehicle or the mSTZ treatment on **(a)** fasting blood glucose (No STZ: n= 20, STZ: n=107; ***P<0.001, unpaired two-sided t-test; t=14.64, df=125), **(b)** pancreatic islets histology (No STZ: 179 islets of n=3 mice, STZ: 182, n=3; ***P<0.001, unpaired two-sided t-test; β: t=11.17, df=359; α: t=10.62, df=357; δ: t=4.203, df=340), **(c)** the insulin positive area within pancreatic sections (No STZ: 27 sections of n=3 mice; STZ: 27, n=3; ***P<0.001, unpaired two-sided t-test; t=3.646, df=52), **(d)** the proliferation (No STZ: 58 islets of n=3 mice; STZ: 69, n=3; ***P<0.001, unpaired two-sided t-test t=1.707, df=125) and **(e)** apoptosis rate in β-cells (No STZ: 46 islets of n=3 mice; STZ: 42, n=3; ***P<0.001, unpaired two-sided t-test, t=3.934, df=86), **(f)** the expression of β-cell functional marker Ucn3 and Glut2 (representative pictures are depicted), **(g)** the homeostatic model assessment of β-cell function (HOMA-β) (No STZ: n= 20, STZ: n=107; ***P<0.001, unpaired two-sided t-test; t=20.24, df=125) and **(h)** the ratio of fasting C-peptide to fasting blood glucose (No STZ: n= 20, STZ: n=106; ***P<0.001, unpaired two-sided t-test; t=12.73, df=124). Boxplots covering all data points are presented. All figures scale bar, 50 μm.

Extended Data Fig. 2

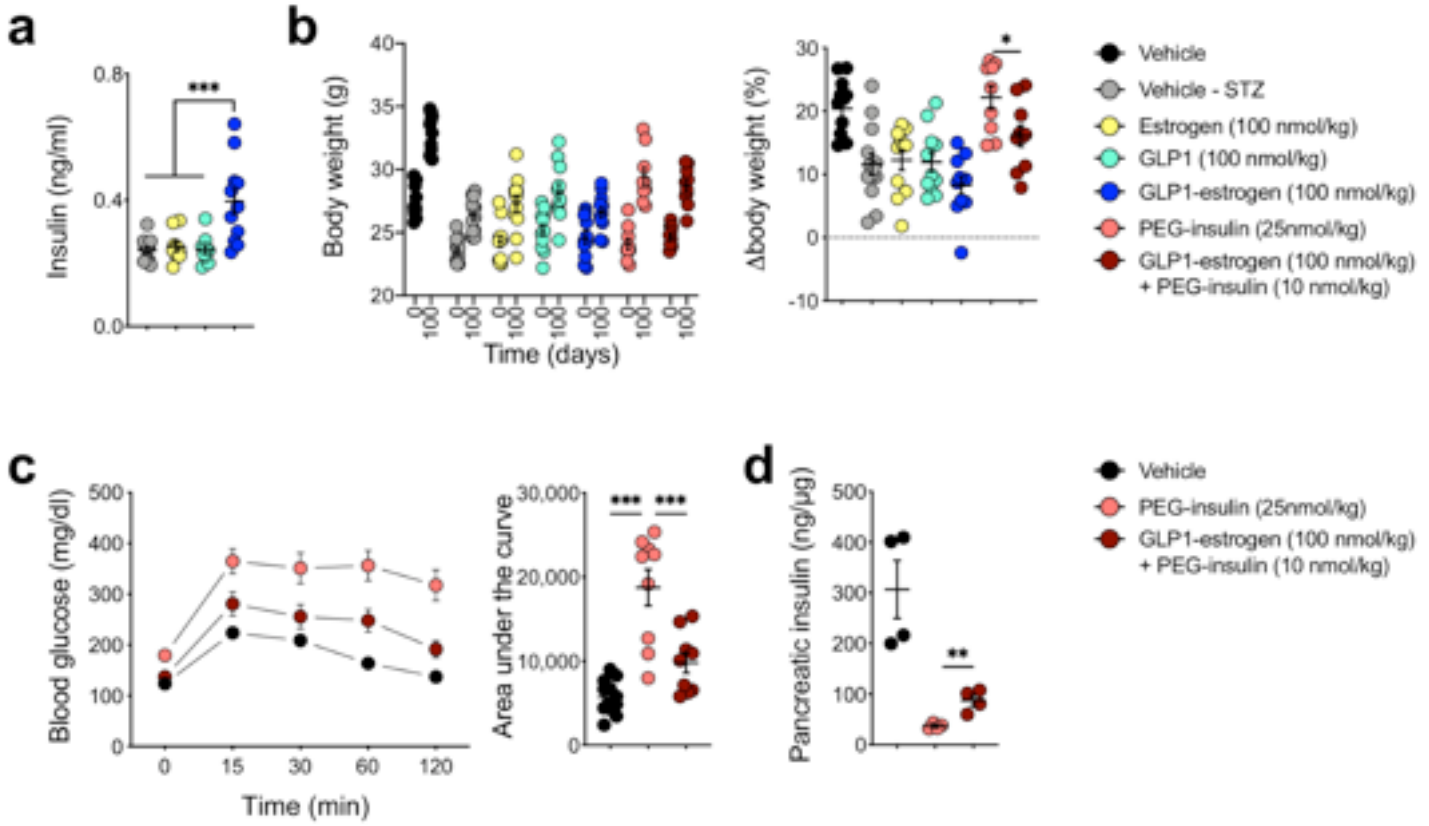

Extended Data Figure 2: Benefits of polypharmcotherapy to ameliorate mSTZ diabetes in mice. Effect of treatment with indicated compounds and doses on **(a)** fasting plasma insulin levels at week 12 of treatment (***P < 0.001, one-way ANOVA with Tukey post-hoc (F (3, 39) = 10.66) and **(b)** body weight in the end of the study (*P < 0.05, unpaired two-sided t-test; t=2.436, df=17). Data are mean ± SEM. **(c-d)** Comparison of PEG-insulin and GLP-1/estrogen plus PEG-insulin co-treated mice. **(c)** Blood glucose after intraperitoneal glucose (0.5g/kg) at week 12 (***P<0.001, one-way ANOVA with Tukey post-hoc (F (2, 27) = 24.71)). **(d)** Pancreatic insulin content in the end of the study (**P<0.01, unpaired two-sided t-test; t=4.534, df=6).

Extended Data Fig. 3

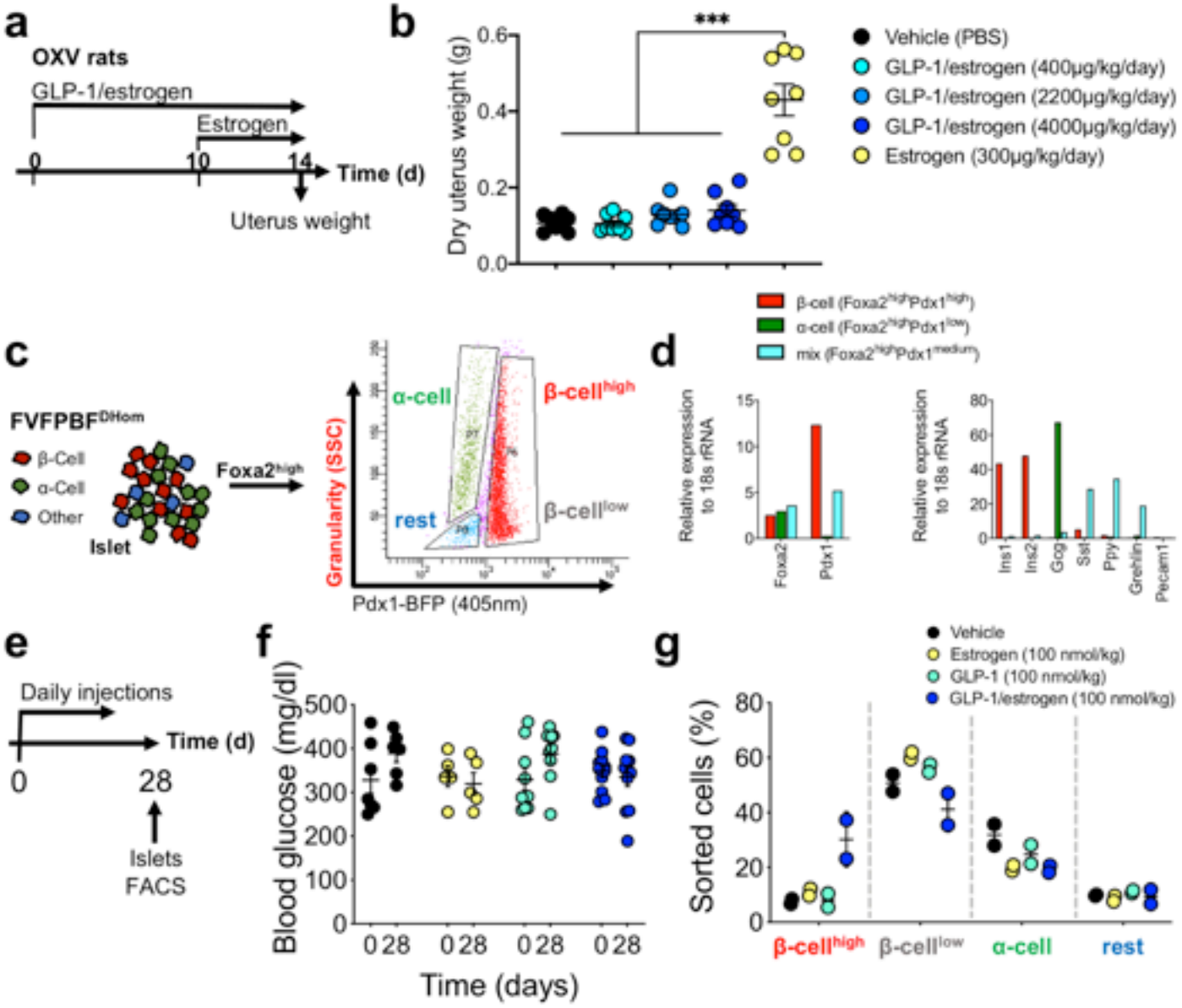

Extended Data Figure 3: Tissue specificity and β-cell selectivity of the GLP-1/estrogen conjugate. (a-b) Treatment of female OVX Sprague-Dawley rats. **(a)** Study scheme. **(b)** Dry uterus weight. Data are mean ± SEM. N=8 female rats per group. ***P < 0.001, one-way ANOVA with Tukey post-hoc (F (4, 35) = 44.18). **(c-h)** Treatment of male FVFPBF^{DHom} mice. **(c)** FACS gating strategy of dispersed endocrine cells based on granularity (Side Scatter Cell (SSC)) and PBF (405 nm) intensity. **(d)** qPCR analysis confirmed sorting strategy of endocrine cells. **(e)** Study scheme; FVFPBF^{DHom} male mice were treated with vehicle (n=7), estrogen (n=5), GLP-1 (n=9), or GLP-1/estrogen (n=11) at the indicated doses for four weeks. **(f)** Fasting blood glucose. Data are mean ± SEM. **(g)** Sorted endocrine cell populations. Individual points represent pancreatic islets of n=2-3 mice per treatment group.

Extended Data Fig. 4

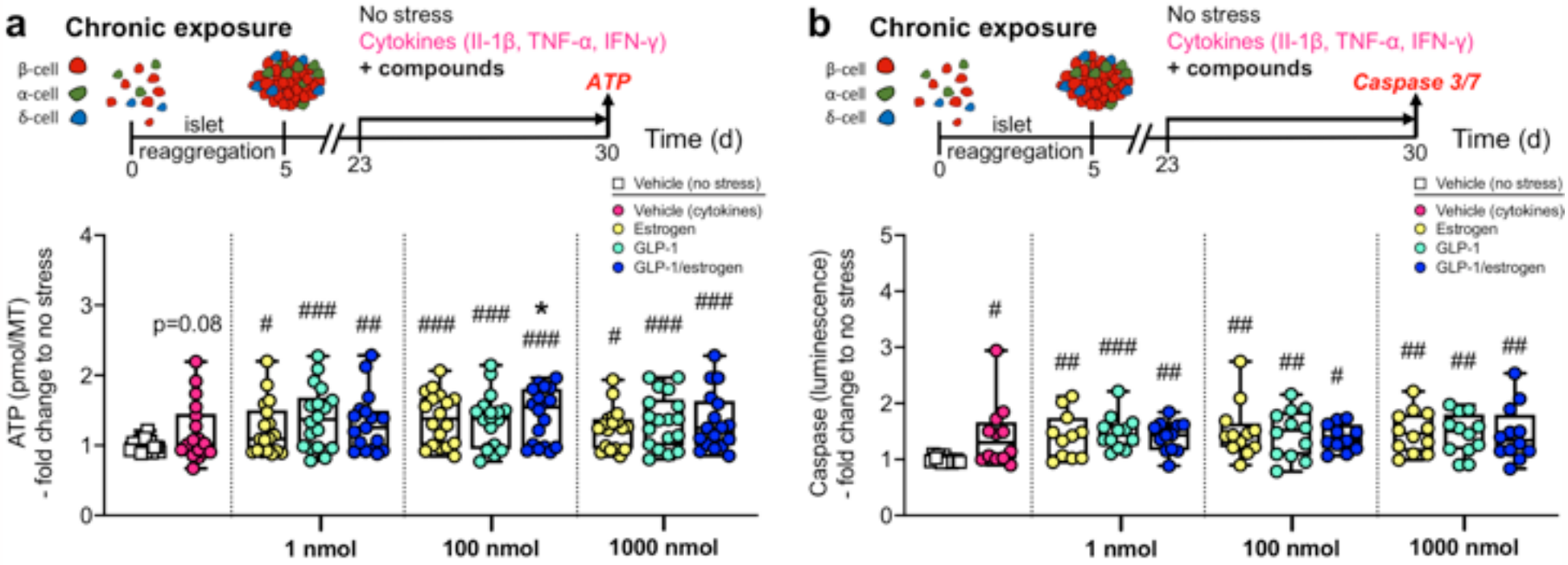

Extended Data Fig. 4: Viability and cell death of human micro-islets. Measurement of human micro-islet viability and cell death with and without cytokine exposure and in the present of different compounds at the indicated doses. **(a)** ATP content and **(b)** Caspase 3/7 activity of human micro-islets. $^{\#}$P<0.05, $^{\#\#}$P<0.01, $^{\#\#\#}$P<0.001, to vehicle (no stress) treatment. *P<0.05, among compound treatments. Significance by one-way ANOVA with donor as random effect followed by Tukey post-hoc. (a) N= 3-4 micro-islets of n=3 human donors for each condition. $F_{low\ dose}(4, 81)= 6.68$; $F_{medium\ dose}(4, 82)=10.68$; $F_{high\ dose}(4, 81)=6.63$. (b) $^{\#}$P<0.05, $^{\#\#}$P<0.01, $^{\#\#\#}$P<0.001. (b) N= 5-6 micro-islets of n=3 human donors for each condition. $F_{low\ dose}(4, 52)= 5.58$; $F_{medium\ dose}(4, 52)=4.44$; $F_{high\ dose}(4, 53)=4.42$.

Extended Data Fig. 5

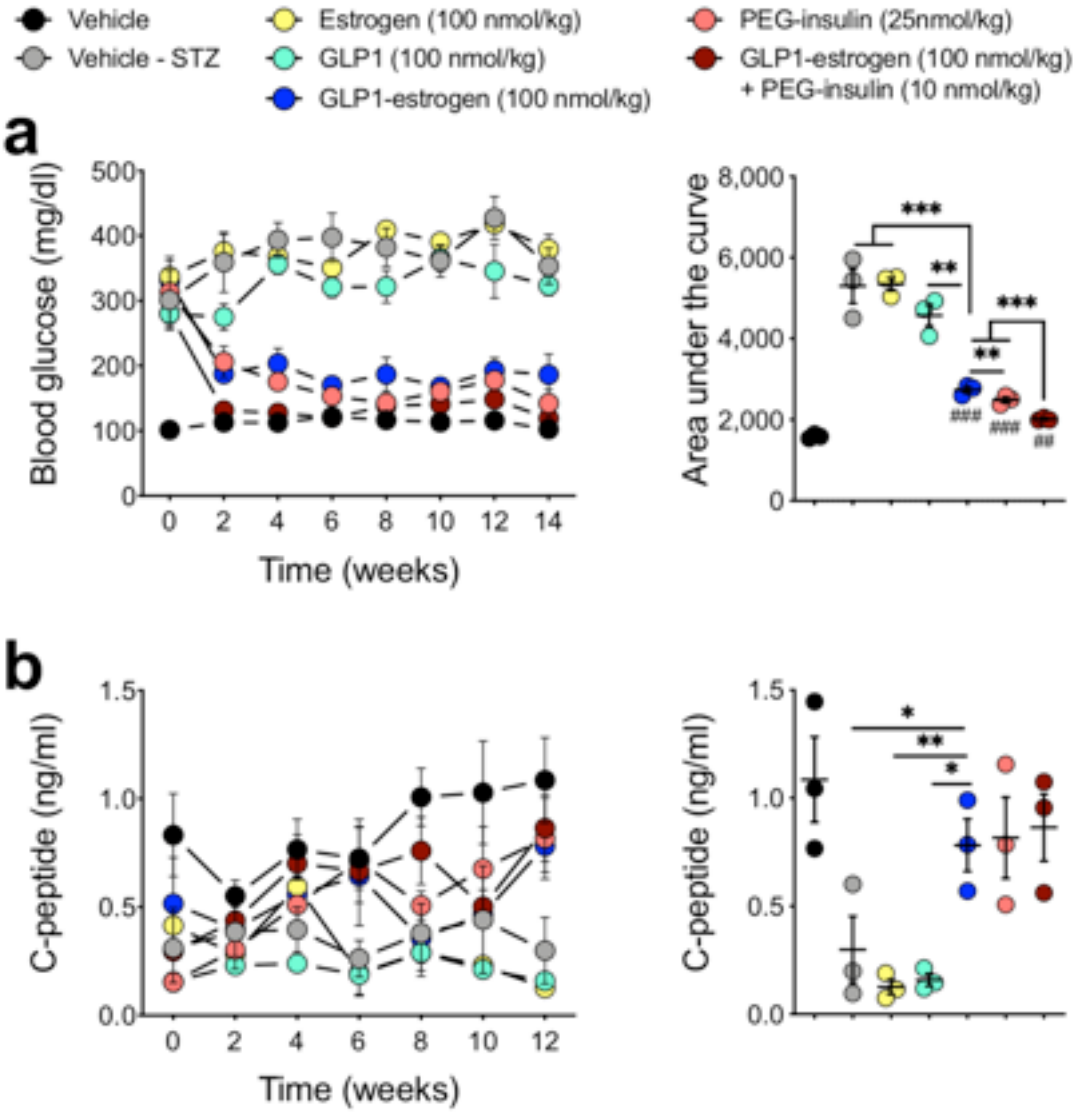

Extended Data Figure 5: Physiological characteristics of mice used for scRNA-seq. Representative mice (n=3) of each treatment were used for scRNA-seq. **(a)** Fasting glucose levels. **P < 0.01, ***P < 0.001, among STZ, estrogen, GLP-1 and GLP-1/estrogen treated mice (one-way ANOVA with Tukey post-hoc test, F (3, 8) = 21.23). *P < 0.01, ***P < 0.001 to compound injections; ##P<0.01, ###P<0.001 to no STZ mice, comparing no STZ, GLP-1/estrogen, PEG-insulin, and co-treated mice (one-way ANOVA with Tukey post-hoc , F (3, 8) = 94.06). **(b)** Fasting C-peptide levels. *P < 0.05, **P < 0.01, among STZ, estrogen, GLP-1, and GLP-1/estrogen treated mice (one-way ANOVA with Tukey post-hoc, F (3, 8) = 9.086). Data are mean ± SEM.

Extended Data Fig. 6

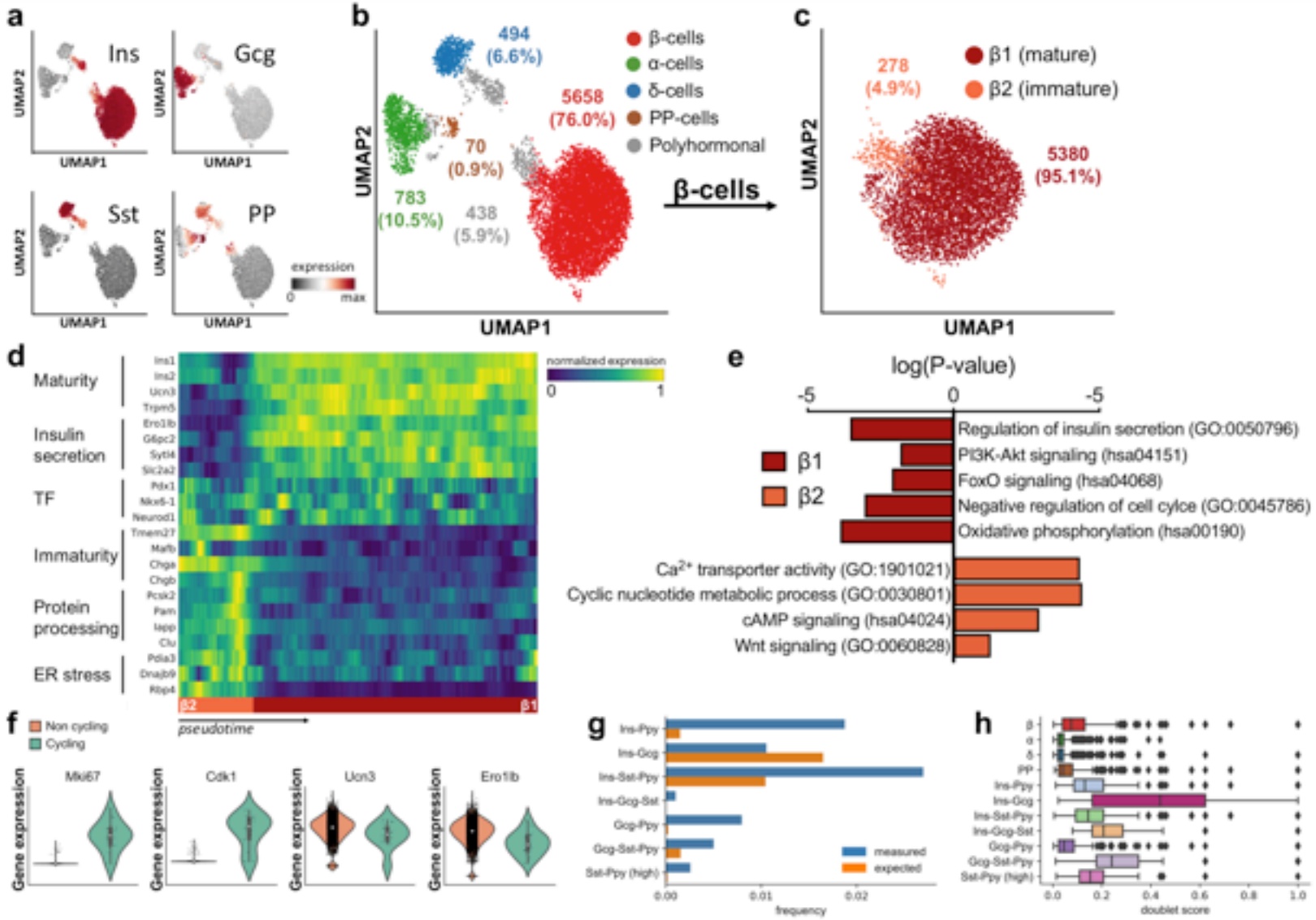

Extended Data Figure 6: β-cell heterogeneity in healthy mice. (a) Endocrine cell annotation is based on the hormone expression of insulin (Ins), glucagon (Gcg), somatostatin (Sst), and pancreatic polypeptide (PP). **(b)** UMAP plot showing all endocrine cells (7578 cells in total) from healthy mice. The cell number and proportion of each endocrine cluster is indicated. **(c)** Redefined clustering of the Ins$^+$β-cells revealed two main β-cell subpopulations. **(d)** Expression changes of genes from selected pathways along a pseudotime trajectory from β2- to β1-cells. β1-cells were downsampled to 1000 cells for better visualization. **(e)** GO term and KEGG pathway enrichment analysis of up- (log fold change>0.25) and downregulated (log fold change<-0.25) genes in β2-cells compared to β1-cells. **(f)** Violin plots showing the distribution of the expression of proliferation and β-cell maturation genes suggesting an immature phenotype of cycling β-cells. Accordingly, 16/403 of the β2-cells, whereas only 2/5319 of the mature β1-cells were classified as cycling (M&M). **(g)** Measured proportion and expected doublet frequency of polyhormonal cell clusters. Expected doublet frequency is calculated given a doublet rate of 10% (M&M). **(h)** Boxplot displaying the doublet score distribution of mono- and polyhormonal cell clusters. A high score indicates a high doublet probability.

Extended Data Fig. 7

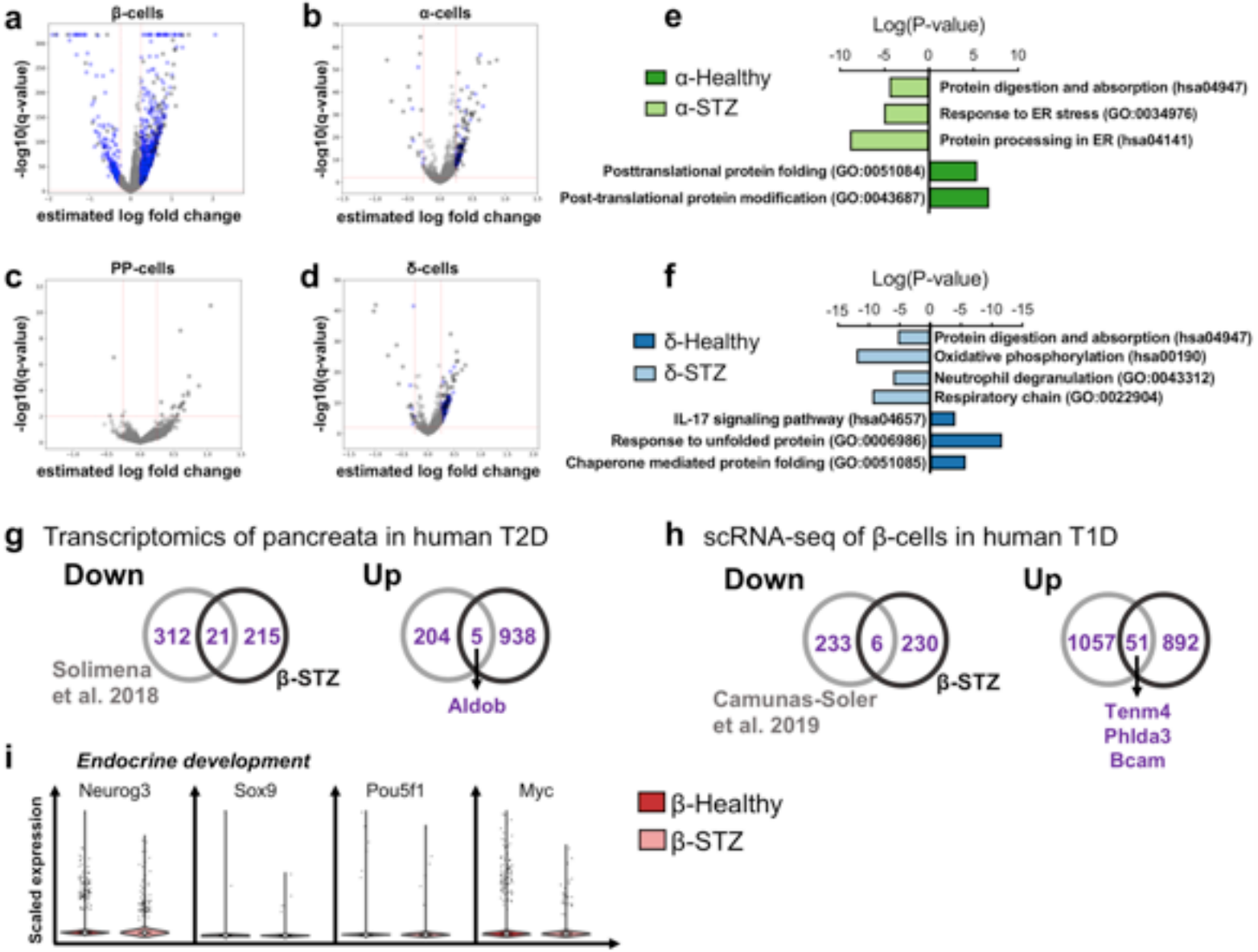

Extended Data Figure 7: Novel β-cell dedifferentiation markers in STZ-diabetic mice. (a – d) Volcano plots showing differential expression and its significance (-log10(adjusted p-Value), limma) for each gene in **(a)** β-, **(b)** α-, **(c)** PP-, and **(d)** δ-cells from mSTZ treated versus healthy mice. Red line indicates thresholds used on significance level and gene expression change. Significantly regulated genes are highlighted in black. Genes significantly regulated in only one cell type but not the others are highlighted in blue. **(e – f)** GO term and KEGG pathway enrichment analysis of up- (log fold change>0.25) and downregulated (log fold change<-0.25) genes in **(e)** α- and **(f)** δ-cells in mSTZ treated versus healthy mice. **(g - h)** Comparison between dysregulated genes in mSTZ β-cells in mice with **(g)** data from RNA-seq of human T2D pancreata and **(h)** from scRNA-seq of human T1D β-cells. Gene names of overlapping genes and identified dedifferentiation markers in Fig. 4e) are listed. **(i)** Violin plots showing the distribution of the expression of endocrine developmental genes in beta cells of mSTZ treated and healthy mice.

Extended Data Fig. 8

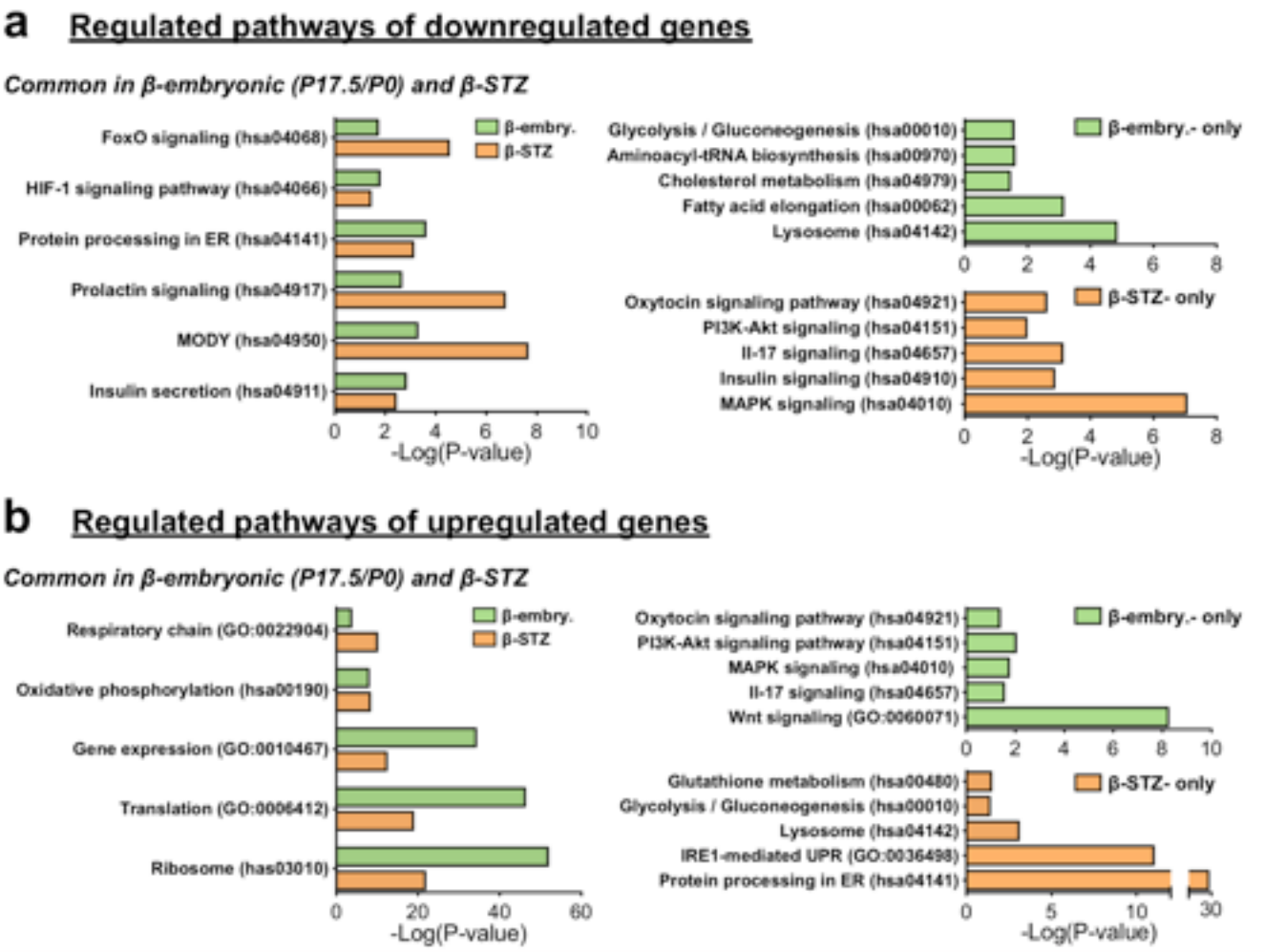

Extended Data Figure 8: Common and distinct genes and pathways of embryonic and dedifferentiated β-cells. Gene ontologies (Pvalue<0.0001) and KEGG pathways (Pvalue<0.05) that are commonly and specifically **(a)** down- and **(b)** upregulated in embryonic and mSTZ-derived β-cells.

Extended Data Fig. 9

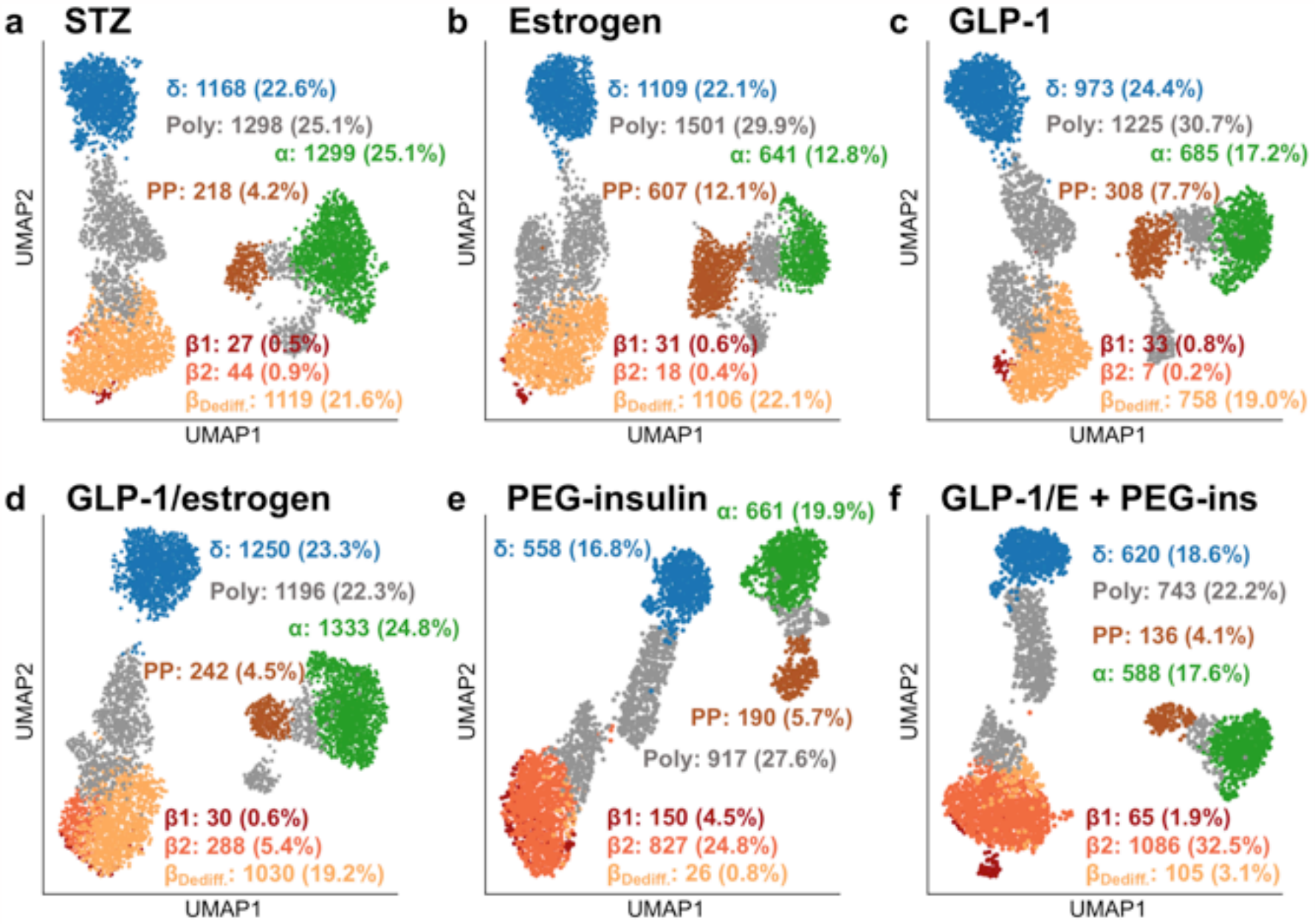

Extended Data Figure 9: Effects on endocrine cells among different treatments. UMAP plot of all endocrine cells after 100 days of treatment showing endocrine cell distribution in each individual treatment. Total cell number for **(a)** mSTZ diabetic mice 5001, for **(b)** estrogen treated mice 4889, for **(c)** GLP-1 treated mice 3874, for **(d)** GLP-1/estrogen treated mice 5201, for **(e)** PEG-insulin treated mice 3217, and for **(f)** GLP-1/estrogen (GLP-1/E) and PEG-insulin (PEG-ins) co-treated mice 3276. Values indicate the proportions of each cell cluster.

Extended Data Fig. 10

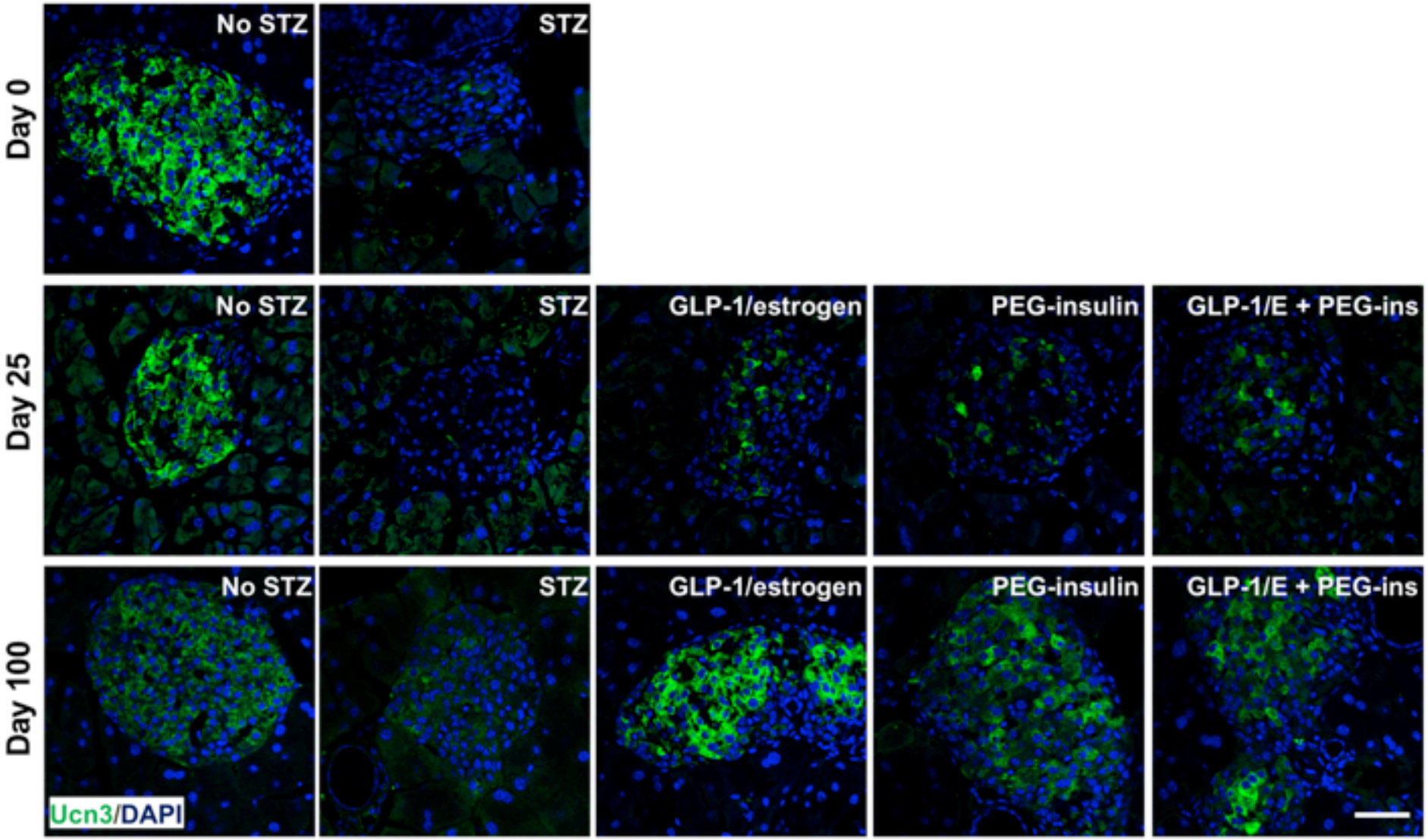

Extended Data Figure 10: β-cell maturation state before and after compound treatment. Immunohistochemical analysis of Ucn3 expression during the course of the study. Scale bar, 50 μm.

Extended Data Fig. 11

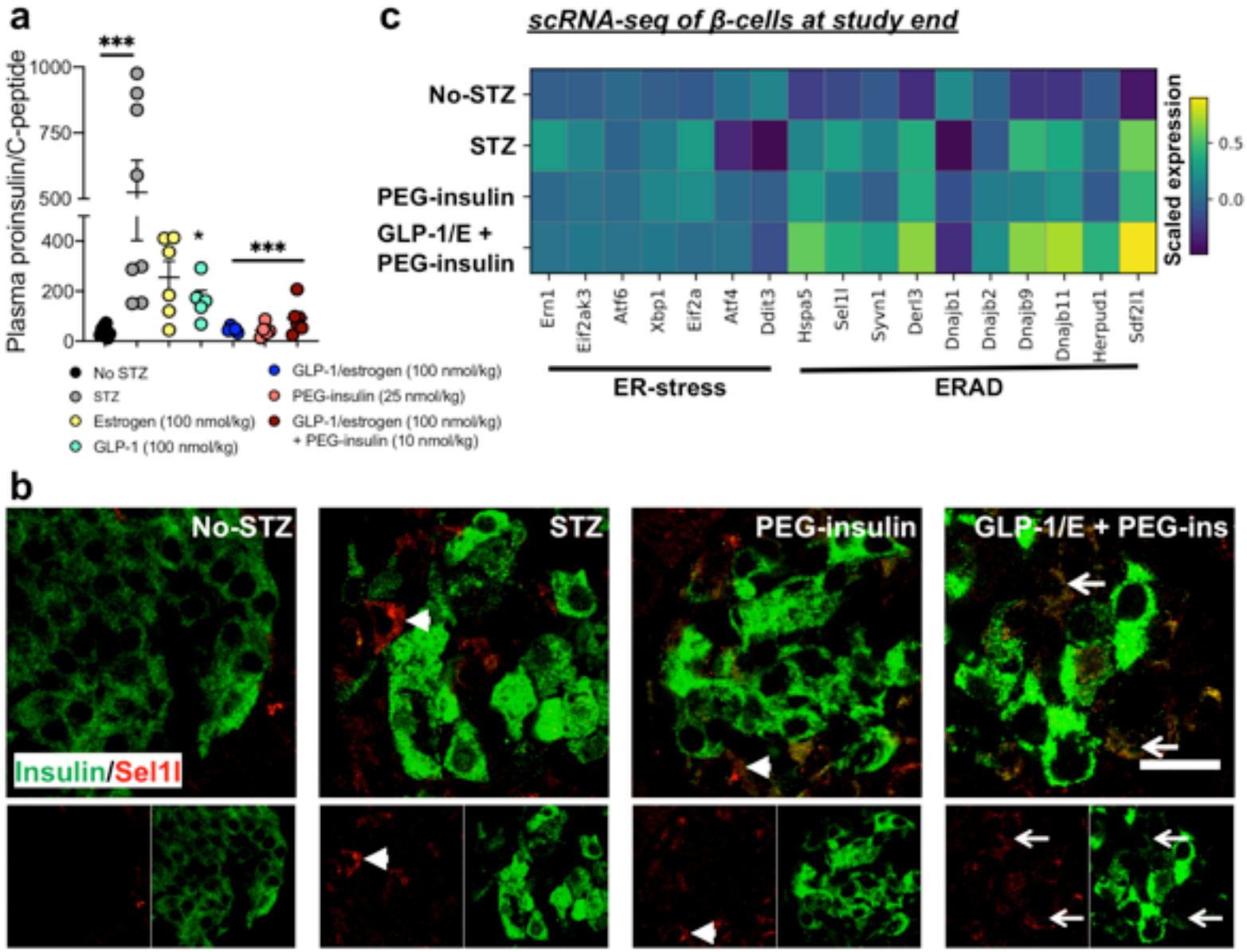

Extended Data Figure 11: β-cell maturation state before and after compound treatment. (a) Plasma proinsulin/C-peptide ration in the end of the study. *P < 0.05, **P < 0.01, ***P < 0.001, by one-way ANOVA followed by Tukey post-hoc (F(6, 36) = 8.12). **(b)** Representative staining for insulin and Sel1l after 25 days of treatment. Arrow indicates Sel1l^{+}insulin^{+}-cells, which were especially found in GLP-1/estrogen and PEG-insulin co-treated mice. Sel1l^{+}insulin^{-}-cells (arrow head) were more common in mSTZ-diabetic and PEG-insulin treated mice. Scale bar, 20μm. **(c)** Expression of selected ER stress and ERAD-associated genes by scRNA-seq at study end.